Supporting Information

Synthesis and Characterization of Oxygen-embedded Quinoidal Pentacene and Nonacene

Yanpei Wang,[†] Shuhai Qiu,[†] Sheng Xie,[†] Long Zhou,[‡] Youhua Hong,[†] Jingjing Chang,[‡] Jishan Wu,[‖] and Zebing Zeng[*,†]

[†]State Key Laboratory of Chemo/Biosensing and Chemometrics, College of Chemistry and Chemical Engineering, Hunan University, Changsha 410082, P. R. China

[‡]State Key Discipline Laboratory of Wide Band Gap Semiconductor Technology, Shaanxi Joint Key Laboratory of Graphene, School of Microelectronics, Xidian University, 2 South Taibai Road, Xi'an, 710071, China

[‖]Department of Chemistry, National University of Singapore, 3 Science Drive 3, 117543, Singapore

Table of Contents

1. General methods

General. ^{1}H NMR data were recorded on a 400 MHz spectrometer at room temperature. All chemical shifts are quoted in ppm, relative to tetramethylsilane, using residual solvent peak as a reference standard. The following abbreviations were used to explain the multiplicities: s = singlet, d = doublet, m = multiplet and "br" represented a broad peak. Absorption spectra were recorded on a Shimadzu UV-3600 plus. Photoluminescence spectra were recorded on a Thermo Scientific Lumina. Absolute fluorescence quantum yields were recorded on a British Edinburgh FLs980 full-function stable and steady-state fluorescence spectrometer. Elemental analysis was carried out on Elementar (Vairo EL).

2. Additional characterization of new compounds

The neutral compounds were prepared as the synthetic procedures described in main text. General procedure for perflurobutoxyl/perflurohexyoyl substituted pentacenes (**P$_1$-PFB** and **P$_1$-PFH**): To the solution of **P$_1$-OH** (1.0 mmol) in dry DMF (40.00 mL), K_2CO_3 and nonafluorobutanesulfonyl fluoride or perfluorohexanesulfonyl fluoride (2.4 mmol) were added. The resulting mixture was stirred overnight at room temperature. After completion of reaction, the solution was diluted with ethyl acetate (200 mL) and water (100 mL), and washed with water (50 mL) several times. Finally, the organic layer was washed with brine (40 mL) and dried by anhydrous Na_2SO_4. After filtration, the organic solvents were evaporated to dryness. The residue was purified by flash column chromatography on silica gel (petroleum ether/tetrahydrofuran = 10:1) to afford corresponding pure compounds. Further crystallization from tetrahydrofuran/menthol afforded molecular materials used in device.

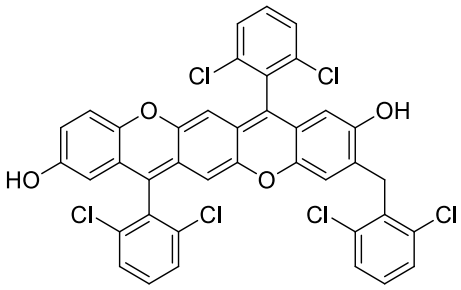

P1-OH was obtained as an amaranth solid. ^{1}H NMR (400 MHz, $CDCl_3$) δ 7.50 (d, *J* = 7.5 Hz, 2H), 7.44 (d, *J* = 6.7 Hz, 2H), 7.37 (t, *J* = 8.3 Hz, 1H), 7.29 - 7.32 (m, 4H), 7.14 (t, *J* = 7.9 Hz, 1H), 6.71 (br, 1H), 6.14 (br, 1H), 5.83 (br, 2H), 5.35 (br, 2H), 4.64: (s, 1H), 4.49 (s, 1H), 4.21 (s, 2H); ^{13}C NMR could not be well-recorded due to its insufficient solubility in various organic solvents and strong intermolecular aggregation as well. Its chemical structure was further confirmed by the single crystal X-ray analysis. HRMS (APCI) *m/z*: calcd for $C_{39}H_{21}Cl_6O_4$ $[M+H]^+$: 762.9555; Found: 762.9566 (error = 1.3 ppm).

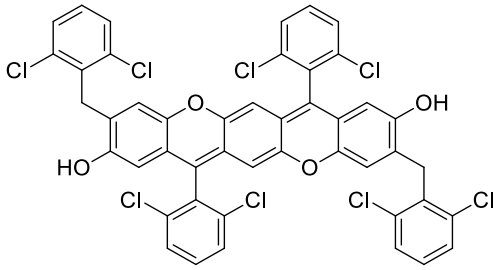

P2-OH was also obtained as an amaranth solid. ^{1}H NMR (400 MHz, THF-d_8) δ 8.20 (s, 2H), 7.55 (d, *J* = 8.0 Hz, 4H), 7.47 - 7.31 (m, 6H), 7.26 - 7.20 (m, 2H), 5.93 (br, 2H), 5.78 (br, 2H), 5.25 (br, 2H), 4.18 (s, 4H). ^{13}C NMR could not be well-recorded because of suffering from similar solubility problem and aggregation issues. **P2-OH** was converted into **P2-OMe**, which was further confirmed. HRMS (APCI) *m/z*: calcd for $C_{46}H_{24}Cl_8O_4$ $[M]^+$: 924.9157; Found: 924.9221 (error = 6.6 ppm).

Compounds N1-OH/N2-OH

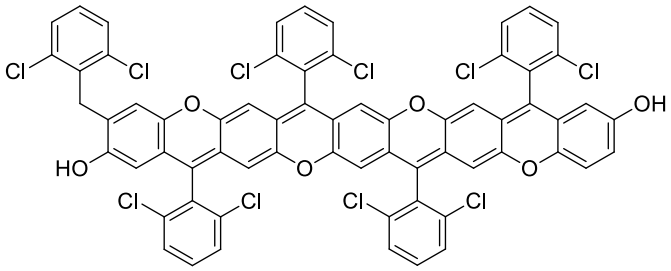

N_1-OH was obtained as a deep blue solid. ^{1}H NMR and ^{13}C NMR could not be recorded due to due to its poor solubility and strong aggregation. HRMS (APCI) *m/z*: calcd for $C_{65}H_{30}Cl_{10}O_6$ $[M]^+$: 1255.8921; Found: 1255.8922 (error = 0.1 ppm).

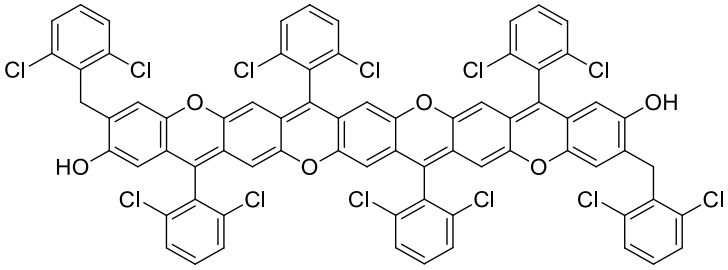

N_2-OH was obtained as a deep blue solid, which is supported by mass spectroscopy and UV-*vis*-NIR spectroscopy as mentioned in main text. HRMS (MALDI-TOF) *m/z*: calcd for $C_{72}H_{34}Cl_{12}O_6$ $[M]^+$: 1419.8501; Found: 1419.8529 (error = 2.0 ppm).

Compounds P_1-OMe, P_2-OMe and N_1-OMe

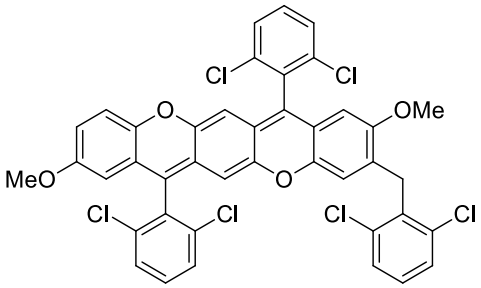

P_1-OMe was obtained as an amaranth solid. ^{1}H NMR (400 MHz, $CDCl_3$) δ 7.52 (d, *J* = 8.0 Hz, 2H), 7.43 (d, *J* = 8.0 Hz, 2H), 7.37 (t, *J* = 8.0 Hz, 1H), 7.31 (d, *J* = 8.0 Hz, 3H), 7.14 (t, *J* = 8.0 Hz, 1H), 6.75 (d, *J* = 8.7 Hz, 1H), 6.59 (br, 1H), 6.09 (s, 1H), 5.87 (d, *J* = 5.4 Hz, 2H), 5.44 (br, 1H), 5.37 (br, 1H), 4.18 (s, 2H), 3.63 (s, 3H), 3.61 (s, 3H). Its chemical structure was confirmed by the single crystal X-ray analysis. HRMS (APCI) *m/z*: calcd for $C_{41}H_{25}Cl_6O_4$ $[M+H]^+$: 790.9860; Found: 790.9879 (error = -2.4 ppm).

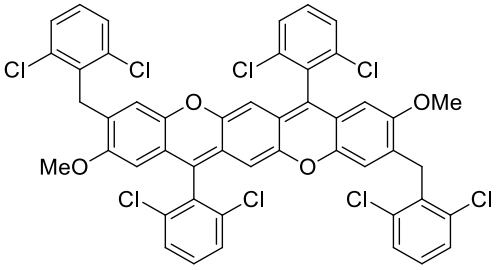

P2-OMe was obtained as an amaranth solid. ^{1}H NMR (400 MHz, $CDCl_3$) δ 7.45 (d, *J* = 7.8 Hz, 4H), 7.30 (d, *J* = 8.0 Hz, 6H), 7.13 (t, *J* = 7.7 Hz, 2H), 6.05 (s, 2H), 5.81 (s, 2H), 5.32 (br, 2H), 4.17 (br, 4H), 3.61 (s, 6H). Its chemical structure was confirmed by the single crystal X-ray analysis. HRMS (APCI) *m/z*: calcd for $C_{48}H_{28}Cl_8O_4$ $[M]^+$: 947.9478; Found: 947.9490 (error = 1.3 ppm).

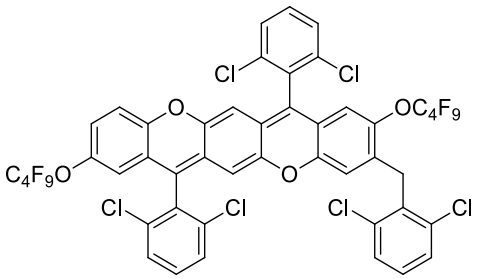

P1-PFB was obtained as an orange solid. ^{1}H NMR (400 MHz, $CDCl_3$) δ 7.52 (d, *J* = 8.0 Hz, 2H), 7.47 (d, *J* = 8.1 Hz, 2H), 7.40 (br, 1H), 7.34 (br, 3H), 7.19 (br, 1H), 6.93 (s, 1H), 6.85 (d, *J* = 8.7 Hz, 1H), 6.30 (s, 1H), 6.22 (d, *J* = 7.5 Hz, 2H), 5.56 (br, 1H), 5.47 (br, 1H), 4.28 (s, 2H). ^{19}F NMR (376 MHz, $CDCl_3$) δ -80.64 (s), -108.61 (s), -120.79 (s), -125.86 (s). ^{13}C NMR could not be well-recorded because of suffering from strong aggregation. MS (MALDI-TOF) *m/z*: calcd for $C_{47}H_{18}Cl_6F_{18}O_4$ $[M]^+$: 1197.9; Found: 1197.2; Anal. Calcd for: C, 46.99; H, 1.51; Found: C, 46.91; H, 1.52.

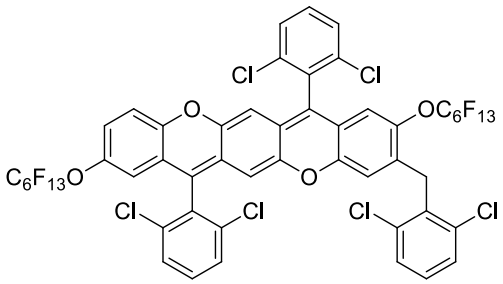

P1-PFH was obtained as an orange solid. ^{1}H NMR (400 MHz, $CDCl_3$) δ 7.52 (d, *J* = 8.0 Hz, 2H), 7.47 (d, *J* = 8.1 Hz, 2H), 7.38-7.42 (br, 1H), 7.35 (br, 2H), 7.33 (br, 1H), 7.17-7.21 (br, 1H), 6.93 (s, 1H), 6.85 (d, *J* = 8.7 Hz, 1H), 6.30 (s, 1H), 6.22 (d, *J* = 7.5

Hz, 2H), 5.56 (br, 1H), 5.47 (br, 1H), 4.28 (s, 2H). ^{19}F NMR (376 MHz, $CDCl_3$) δ -80.68 (s), -108.45 (s), -119.92 (s), -121.64 (s), -122.60 (s), -126.02 (s). ^{13}C NMR could not be well-recorded because of suffering from strong aggregation. MS (MALDI-TOF) *m/z*: calcd for $C_{51}H_{18}Cl_6F_{26}O_4$ $[M]^+$: 1397.9; Found: 1397.3; Anal. Calcd for: C, 43.71; H, 1.29; Found: C, 43.69; H, 1.30.

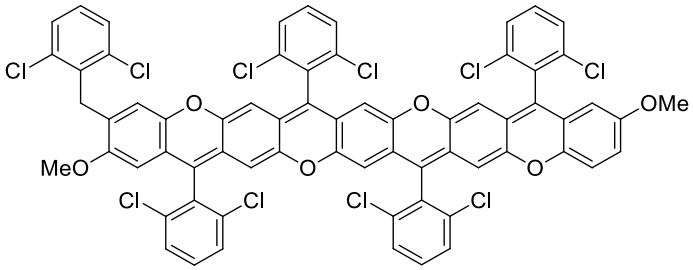

N$_1$-OMe was obtained as a deep blue solid. ^{1}H NMR (400 MHz, THF-d_8) δ 7.56 (m, 8H), 7.50 - 7.44 (m, 3H), 7.41 (d, J = 8.8 Hz, 3H), 7.27 (d, J = 7.6 Hz, 1H), 6.80 (d, J = 8.7 Hz, 1H), 6.68 (br, 1H), 6.03 (s, 1H), 5.94 (s, 1H), 5.91 (s, 1H), 5.77 (s, 2H), 5.44 (s, 1H), 5.33 (br, 3H), 4.19 (s, 2H), 3.58 (s, 6H). Its chemical structure was confirmed by the single crystal X-ray analysis. HRMS (APCI) *m/z*: calcd for $C_{67}H_{34}Cl_{10}O_6$ $[M]^+$: 1288.9215; Found: 1288.9257 (error = 3.2 ppm).

3. Reaction optimization and proposed reaction mechanism

To obtain optimized reaction condition, the cross-condensation reaction was conducted under several conditions. General procedure: a solution of hydroquinone (100 mg, 1.82 mmol) and 2,6-dichlorobenzaldehyde (158 mg, 1.82 mmol) in acetic acid (15 mL) or in mixed solvent of acetic acid and xylene, was purged with nitrogen for 10 min. To the reaction mixture, a catalyst amount of concentrated hydrochloric acid or concentrated sulfuric acid or boron trifluoride diethyl etherate was added slowly. The mixture was heated to reflux under inert atmosphere, and the reaction was monitored by thin layer chromatography (TLC). After reaction quenching and treatment of the crude solid, the product was isolated by chromatography on silica gel.

Reaction condition screening

Entry	Conditions	Results (yield)
1	Con.HCl (cat.), AcOH, 127 ℃, 72 h	**P_1-OH** (~25%), **P_2-OH** (trace)
3	BF_3•$(OEt)_2$ (cat.), AcOH, 127 ℃, 168 h	trace
4	Con.H_2SO_4 (cat.), AcOH, 127 ℃, 20 h	**P_1-OH** (54%), **P_2-OH** (16%), **N_1-OH** (trace)
5	Con.H_2SO_4 (cat.), AcOH/xylene, 140 ℃, 30 h	**N_1-O**H (37%), **N_2-OH** (1%)

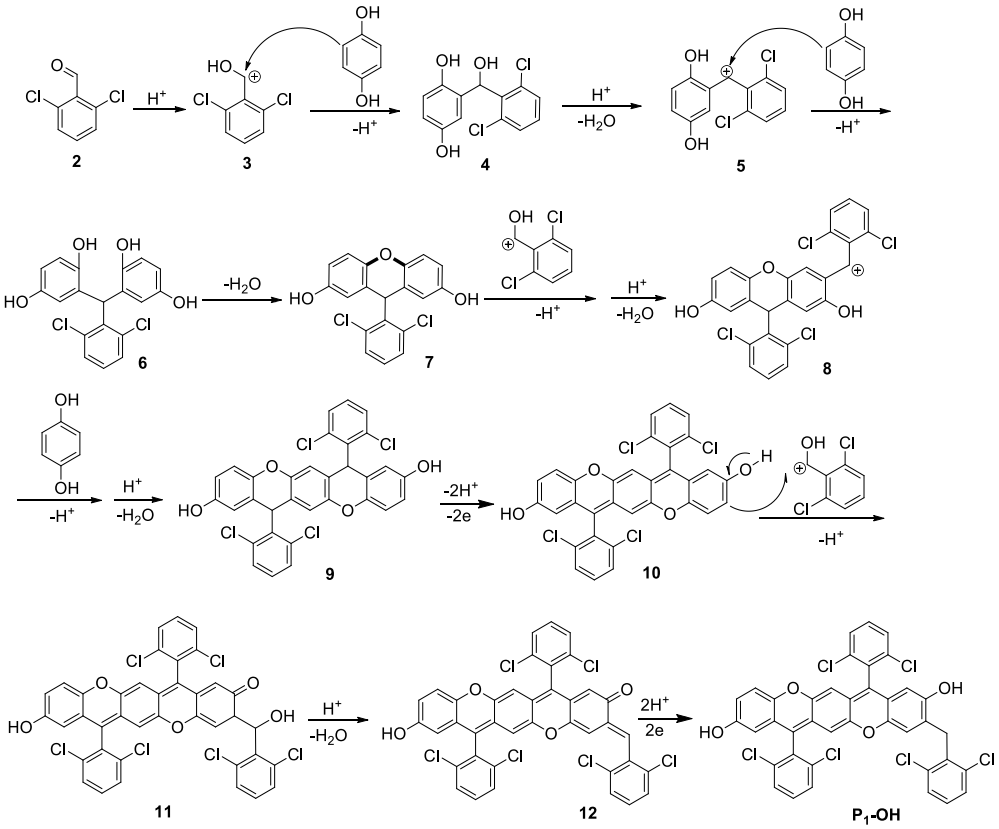

Scheme S1. Proposed reaction mechanism for O-doping pentacene **P_1-OH**.

4. Single-crystal X-Ray analysis

4.1 Crystallographic data for P_2-OH

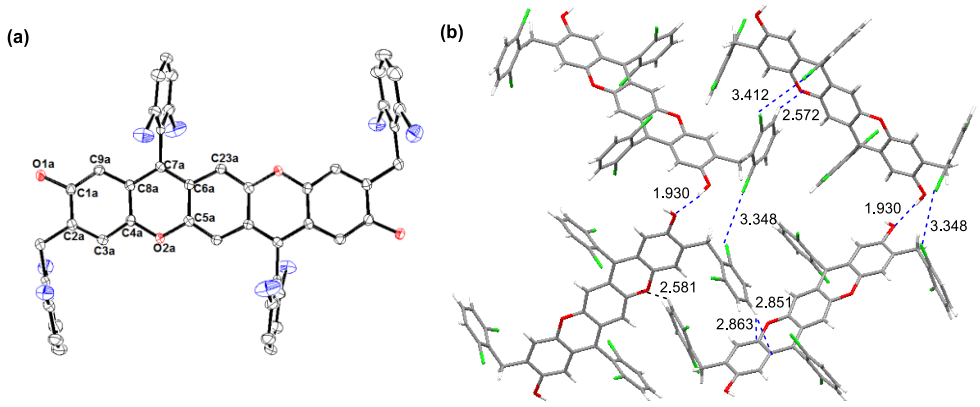

Figure S1. Crystal structures (thermal ellipsoids are shown at 30%) of **P_2-OH** (a) and molecular packing features via intermolecular hydrogen/halogen interactions (b).

Table S1. Crystal data and structure refinement for **P_2-OH**.

Identification code	**P_2-OH**
Empirical formula	$C_{46}H_{24}Cl_8O_4$
Formula weight	996.35
Temperature/K	100(2)
Crystal system	monoclinic
Space group	$P2_1/c$
a/Å	24.2970(13)
b/Å	7.8094(4)
c/Å	23.9522(12)
α/°	90
β/°	98.529(2)
γ/°	90
Volume/Å^3	4494.5(4)
Z	4
ρ_{calc}g/cm^3	1.472
μ/mm^{-1}	4.980

F(000)	2032
Crystal size/mm^3	0.366 × 0.123 × 0.122
2Θ range for data collection/°	3.679 to 68.241
Index ranges	$-27 \leq h \leq 29$, $-9 \leq k \leq 9$, $-28 \leq l \leq 27$
Reflections collected	45841
Independent reflections	8241 [R_{int} = 0.0452]
Data/restraints/parameters	8241/40/617
Goodness-of-fit on F^2	1.064
Final R indexes [I>=2σ (I)]	R_1 = 0.0464, wR_2 = 0.1138
Final R indexes [all data]	R_1 = 0.0532, wR_2 = 0.1181
Largest diff. peak/hole / e Å^{-3}	0.544/-0.535

Table S2. Bond lengths [Å] for **P_2-OH**.

Cl(1A)-C(12A)	1.749(3)	C(4B)-C(8B)	1.397(4)
Cl(3A)-C(22A)	1.735(3)	C(5B)-C(6B)	1.443(3)
O(1A)-C(1A)	1.370(3)	C(6B)-C(23B)	1.429(3)
O(2A)-C(5A)	1.371(3)	C(7B)-C(17B)	1.489(3)
C(1A)-C(9A)	1.388(3)	C(9B)-H(9B)	0.9500
C(2A)-C(3A)	1.390(3)	C(0B)-H(10C)	0.9900
C(3A)-C(4A)	1.381(3)	C(11B)-C(12B)	1.388(4)
C(4A)-C(8A)	1.396(3)	C(12B)-C(13B)	1.389(4)
C(5A)-C(6A)	1.440(3)	C(13B)-H(13B)	0.9500
C(6A)-C(23A)	1.432(3)	C(14B)-H(14B)	0.9500
C(7A)-C(17A)	1.489(3)	C(15B)-H(15B)	0.9500
C(9A)-H(9A)	0.9500	C(17B)-C(22B)	1.398(4)
C(10A)-H(10A)	0.9900	C(19B)-C(20B)	1.384(4)
C(11A)-C(12A)	1.386(4)	C(20B)-C(21B)	1.378(4)
C(12A)-C(13A)	1.383(4)	C(21B)-C(22B)	1.390(4)

C(13A)-H(13A)	0.9500	C(23B)-C(5B)#2	1.351(4)
C(14A)-H(14A)	0.9500	O(1S)-C(1S)	1.459(6)
C(15A)-H(15A)	0.9500	C(1S)-C(2S)	1.459(6)
C(17A)-C(22A)	1.391(3)	C(1S)-H(1S2)	0.9900
C(19A)-C(20A)	1.371(4)	C(2S)-H(2S1)	0.9900
C(20A)-C(21A)	1.379(5)	C(3S)-C(4S)	1.498(8)
C(21A)-C(22A)	1.392(4)	C(3S)-H(3S2)	0.9900
C(23A)-C(5A)#1	1.357(3)	C(4S)-H(4S2)	0.9900
Cl(1B)-C(12B)	1.742(3)	O(1T)-C(4T)	1.463(6)
Cl(3B)-C(22B)	1.738(3)	C(1T)-H(1T1)	0.9900
O(1B)-C(1B)	1.380(3)	C(2T)-C(3T)	1.457(7)
O(2B)-C(5B)	1.366(3)	C(2T)-H(2T2)	0.9900
C(1B)-C(9B)	1.381(3)	C(3T)-H(3T1)	0.9900
C(2B)-C(3B)	1.386(4)	C(4T)-H(4T1)	0.9900
C(3B)-C(4B)	1.375(3)		

4.2 Crystallographic data for P_1-OMe

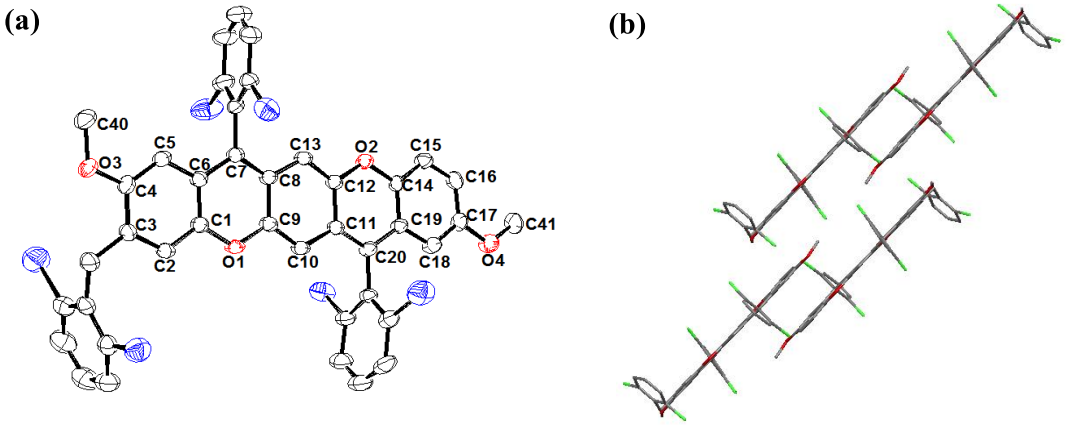

Figure S2. Crystal structures (thermal ellipsoids are shown at 30%; hydrogen atoms are omitted for clarity) of **P_1-OMe** and its packing (b).

Table S3. Crystal data and structure refinement for **P_1-OMe**.

Identification code	**P_1-OMe**

Empirical formula	$C_{41}H_{24}Cl_6O_4$
Formula weight	793.30
Temperature/K	296(2)
Crystal system	monoclinic
Space group	$P2_1/n$
a/Å	10.195(4)
b/Å	13.289(7)
c/Å	16.613(8)
α/°	73.338(15)
β/°	86.579(14)
γ/°	84.425(14)
Volume/Å^3	2144.8(18)
Z	2
ρ_{calc}g/cm^3	1.228
μ/mm^{-1}	0.437
F(000)	808
Crystal size/mm^3	0.200 x 0.160 x 0.130
2Θ range for data collection/°	1.747 to 24.999
Index ranges	-12<=h<=12, -15<=k<=15, -19<=l<=19
Reflections collected	28434
Independent reflections	7455 [R(int) = 0.0952]
Max. and min. transmission	0.7456 and 0.4904
Completeness to theta = 25.242°	96.2
Absorption correction	Semi-empirical from equivalent
Refinement method	Full-matrix least-squares on F^2
Data/restraints/parameters	7455 / 0 / 463
Goodness-of-fit on F^2	1.026

Final R indexes [I>=2σ (I)]	R_1 = 0.0835, wR_2 = 0.2171
Final R indexes [all data]	R_1 = 0.1317, wR_2 = 0.2528
Largest diff. peak/hole / e Å^{-3}	0.515/-0.334

Table S4. Bond lengths [Å] for **P_1-OMe.**

Cl(1)-C(28)	1.739(5)	C(17)-C(18)	1.392(6)
Cl(2)-C(32)	1.721(6)	C(18)-C(19)	1.404(6)
Cl(3)-C(35)	1.746(6)	C(18)-H(18)	0.93
Cl(4)-C(39)	1.732(5)	C(19)-C(20)	1.444(5)
Cl(5)-C(26)	1.736(5)	C(20)-C(21)	1.479(5)
Cl(6)-C(22)	1.730(5)	C(21)-C(26)	1.381(6)
O(1)-C(9)	1.362(5)	C(21)-C(22)	1.402(6)
O(1)-C(1)	1.387(5)	C(22)-C(23)	1.390(7)
O(2)-C(12)	1.368(5)	C(23)-C(24)	1.336(8)
O(2)-C(14)	1.394(4)	C(23)-H(23)	0.93
O(3)-C(4)	1.353(5)	C(24)-C(25)	1.361(8)
O(3)-C(40)	1.419(6)	C(24)-H(24)	0.93
O(4)-C(17)	1.362(5)	C(25)-C(26)	1.423(7)
O(4)-C(41)	1.409(6)	C(25)-H(25)	0.93
C(1)-C(2)	1.362(6)	C(27)-C(32)	1.392(6)
C(1)-C(6)	1.385(6)	C(27)-C(28)	1.392(6)
C(2)-C(3)	1.382(6)	C(28)-C(29)	1.371(7)
C(2)-H(2)	0.93	C(29)-C(30)	1.358(9)
C(3)-C(4)	1.411(6)	C(29)-H(29)	0.93
C(3)-C(33)	1.504(6)	C(30)-C(31)	1.361(9)
C(4)-C(5)	1.385(6)	C(30)-H(30)	0.93
C(5)-C(6)	1.396(5)	C(31)-C(32)	1.402(7)
C(5)-H(5)	0.93	C(31)-H(31)	0.93
C(6)-C(7)	1.451(6)	C(33)-C(34)	1.513(6)

C(7)-C(8)	1.375(5)	C(33)-H(33A)	0.97
C(7)-C(27)	1.492(6)	C(33)-H(33B)	0.97
C(8)-C(13)	1.418(6)	C(34)-C(39)	1.371(6)
C(8)-C(9)	1.441(6)	C(34)-C(35)	1.410(7)
C(9)-C(10)	1.353(6)	C(35)-C(36)	1.356(8)
C(10)-C(11)	1.432(6)	C(36)-C(37)	1.359(9)
C(10)-H(10)	0.93	C(36)-H(36)	0.93
C(11)-C(20)	1.367(5)	C(37)-C(38)	1.351(8)
C(11)-C(12)	1.442(5)	C(37)-H(37)	0.93
C(12)-C(13)	1.353(5)	C(38)-C(39)	1.399(7)
C(13)-H(13)	0.93	C(38)-H(38)	0.93
C(14)-C(15)	1.369(6)	C(40)-H(40A)	0.96
C(14)-C(19)	1.383(5)	C(40)-H(40B)	0.96
C(15)-C(16)	1.372(6)	C(40)-H(40C)	0.96
C(15)-H(15)	0.93	C(41)-H(41A)	0.96
C(16)-C(17)	1.382(6)	C(41)-H(41B)	0.96
C(16)-H(16)	0.93	C(41)-H(41C)	0.96

4.3 Crystallographic data for P_2-OMe

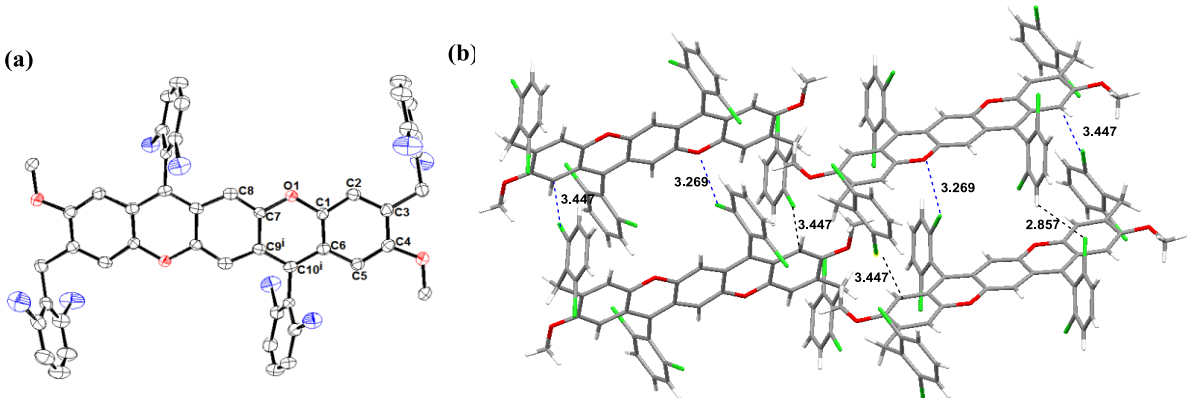

Figure S3. Crystal structures (thermal ellipsoids are shown at 30%) of **P_2-OMe** (a) and its packing diagrams (b).

Table S5. Crystal data and structure refinement for **P_2-OMe**.

dentification code	**P_2-OMe**
Empirical formula	$C_{48}H_{28}Cl_8O_4$
Formula weight	952.30
Temperature/K	173
Crystal system	monoclinic
Space group	$P2_1/c$
a/Å	11.333(2)
b/Å	7.4415(15)
c/Å	25.055(6)
α/°	90
β/°	92.183(7)
γ/°	90
Volume/Å^3	2111.4(8)
Z	2
ρ_{calc}g/cm^3	1.498
μ/mm^{-1}	0.580
F(000)	968
Crystal size/mm^3	0.100 × 0.060 × 0.040
2Θ range for data collection/°	1.627 to 24.999
Index ranges	$-13 \leq h \leq 13$, $-8 \leq k \leq 8$, $-29 \leq l \leq 29$
Reflections collected	21183
Independent reflections	3690 [R_{int} = 0.1175]
Completeness to theta = 25.242°	96.6 %
Absorption correction	Semi-empirical from equivalents
Max. and min. transmission	0.7456 and 0.4575
Refinement method	Full-matrix least-squares on F2
Data/restraints/parameters	3690/0/272

Goodness-of-fit on F^2	1. 090
Final R indexes [I>=2σ (I)]	R_1 = 0.0794, wR_2 = 0.2006
Final R indexes [all data]	R_1 = 0.1133, wR_2 = 0.2260
Largest diff. peak/hole / e $Å^{-3}$	0.458/-0.721

Table S6. Bond lengths [Å] for **P_2-OMe**.

Cl(1)-C(12)	1.729(6)	C(10)-C(11)	1.490(7)
Cl(2)-C(16)	1.735(6)	C(11)-C(12)	1.388(7)
Cl(3)-C(19)	1.731(6)	C(11)-C(16)	1.399(7)
Cl(4)-C(23)	1.742(6)	C(12)-C(13)	1.396(8)
O(1)-C(7)	1.367(6)	C(13)-C(14)	1.362(9)
O(1)-C(1)	1.378(6)	C(13)-H(13)	0.95
O(2)-C(4)	1.380(6)	C(14)-C(15)	1.378(9)
O(2)-C(24)	1.425(6)	C(14)-H(14)	0.95
C(1)-C(2)	1.388(7)	C(15)-C(16)	1.378(8)
C(1)-C(6)	1.396(7)	C(15)-H(15)	0.95
C(2)-C(3)	1.388(8)	C(17)-C(18)	1.516(7)
C(2)-H(2)	0.95	C(17)-H(17A)	0.99
C(3)-C(4)	1.410(7)	C(17)-H(17B)	0.99
C(3)-C(17)	1.518(7)	C(18)-C(19)	1.383(8)
C(4)-C(5)	1.371(8)	C(18)-C(23)	1.387(8)
C(5)-C(6)	1.415(7)	C(19)-C(20)	1.396(8)
C(5)-H(5)	0.95	C(20)-C(21)	1.381(9)
C(6)-C(10)#1	1.452(7)	C(20)-H(20)	0.95
C(7)-C(8)	1.347(7)	C(21)-C(22)	1.360(10)
C(7)-C(9)#1	1.454(7)	C(21)-H(21)	0.95
C(8)-C(9)	1.428(7)	C(22)-C(23)	1.381(8)
C(8)-H(8)	0.95	C(22)-H(22)	0.95
C(9)-C(10)	1.380(7)	C(24)-H(24A)	0.98

C(9)-C(7)#1	1.454(7)	C(24)-H(24B)	0.98
C(10)-C(6)#1	1.452(7)	C(24)-H(24C)	0.98

4.4 Crystallographic data for N_1-OMe

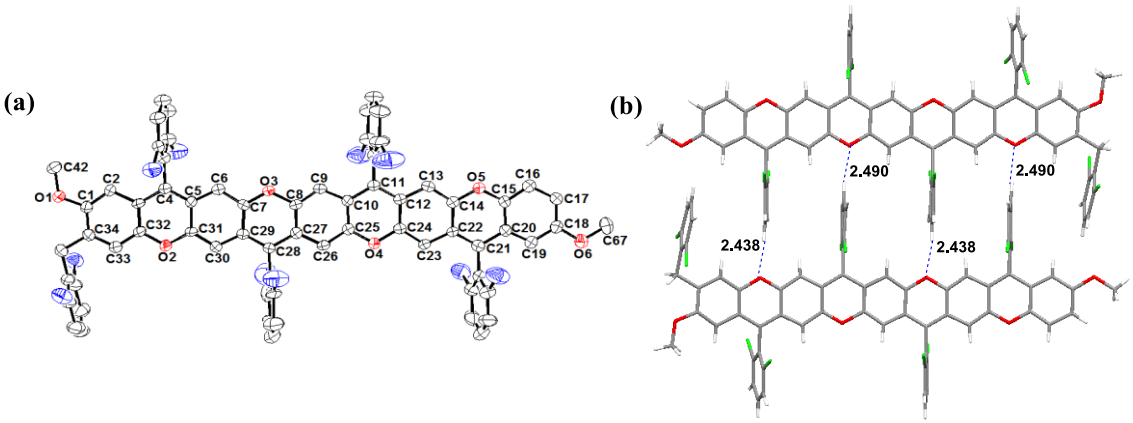

Figure S4. Crystal structures (thermal ellipsoids are shown at 30%) of **N_1-OMe** (a) and its packing diagrams (b).

Table S7. Crystal data and structure refinement for **N_1-OMe**.

Identification code	**N_1-OMe**
Empirical formula	$C_{67}H_{34}Cl_{10}O_6$
Formula weight	1289.44
Temperature/K	170.01
Wavelength	1.34139
Crystal system	Triclinic
Space group	P-1
a/Å	11.5455(12)
b/Å	18.2487(17)
c/Å	22.786(2)
α/°	107.665(6)
β/°	96.056(7)
γ/°	96.264(7)
Volume/Å^3	4498.1(8)

Z	2
ρ_{cal}Mg/cm^3	0.952
μ/mm^{-1}	0.075
F(000)	1308
Crystal size/mm^3	0.15 x 0.1 x 0.01
2Θ range for data collection/°	3.280 to 55.343
Index ranges	-12<=h<=14, -22<=k<=22, -27<=l<=27
Reflections collected	53216
Independent reflections	16979 [R(int) = 0.0975]
Completeness to theta = 53.594°	99.4 %
Absorption correction	Semi-empirical from equivalents
Max. and min. transmission	0.7508 and 0.4559
Refinement method	Full-matrix least-squares on F^2
Data/restraints/parameters	16979 / 0 / 750
Goodness-of-fit on F^2	0.834
Final R indexes [I>=2σ (I)]	R_1 =0.1280, wR_2 = 0.3000
Final R indexes [all data]	R_1 = 0.2021, wR_2 = 0.3547
Extinction coefficient	n/a
Largest diff. peak/hole / e Å^{-3}	1.158/-0.532

Table S8. Bond lengths [Å] for **N₁-OMe**.

Cl(1)-C(41)	1.714(9)	C(26)-C(27)	1.387(9)
Cl(2)-C(37)	1.730(9)	C(27)-C(28)	1.458(9)
Cl(3)-C(44)	1.714(10)	C(28)-C(29)	1.392(9)
Cl(4)-C(48)	1.731(8)	C(28)-C(49)	1.574(12)
Cl(5)-C(54)	1.844(12)	C(29)-C(30)	1.395(9)
Cl(6)-C(50)	1.533(10)	C(30)-H(30)	0.95
Cl(7)-C(56)	1.720(11)	C(30)-C(31)	1.355(9)

Cl(8)-C(60)	1.731(11)	C(32)-C(33)	1.369(9)
Cl(9)-C(66)	1.762(9)	C(33)-H(33)	0.95
Cl(10)-C(62)	1.729(9)	C(33)-C(34)	1.381(9)
O(1)-C(1)	1.370(8)	C(34)-C(35)	1.517(9)
O(1)-C(42)	1.427(8)	C(35)-H(35A)	0.99
O(2)-C(31)	1.367(8)	C(35)-H(35B)	0.99
O(2)-C(32)	1.395(8)	C(35)-C(36)	1.551(9)
O(3)-C(7)	1.331(8)	C(36)-C(37)	1.437(11)
O(3)-C(8)	1.425(8)	C(36)-C(41)	1.362(11)
O(4)-C(24)	1.374(8)	C(37)-C(38)	1.390(11)
O(4)-C(25)	1.377(8)	C(38)-H(38)	0.95
O(5)-C(14)	1.370(8)	C(38)-C(39)	1.391(13)
O(5)-C(15)	1.377(8)	C(39)-H(39)	0.95
O(6)-C(18)	1.403(9)	C(39)-C(40)	1.346(13)
O(6)-C(67)	1.392(9)	C(40)-H(40)	0.95
C(1)-C(2)	1.393(9)	C(40)-C(41)	1.407(11)
C(1)-C(34)	1.376(9)	C(42)-H(42A)	0.98
C(2)-H(2)	0.95	C(42)-H(42B)	0.98
C(2)-C(3)	1.452(9)	C(42)-H(42C)	0.98
C(3)-C(4)	1.449(9)	C(43)-C(44)	1.377(11)
C(3)-C(32)	1.385(8)	C(43)-C(48)	1.397(11)
C(4)-C(5)	1.367(9)	C(44)-C(45)	1.428(11)
C(4)-C(43)	1.510(9)	C(45)-H(45)	0.95
C(5)-C(6)	1.400(9)	C(45)-C(46)	1.291(12)
C(5)-C(31)	1.464(9)	C(46)-H(46)	0.95
C(6)-H(6)	0.95	C(46)-C(47)	1.395(13)
C(6)-C(7)	1.388(10)	C(47)-H(47)	0.95
C(7)-C(29)	1.438(9)	C(47)-C(48)	1.370(9)
C(8)-C(9)	1.357(9)	C(49)-C(50)	1.472(14)

C(8)-C(27)	1.395(9)	C(49)-C(54)	1.267(14)
C(9)-H(9)	0.95	C(50)-C(51)	1.448(11)
C(9)-C(10)	1.383(9)	C(51)-H(51)	0.95
C(10)-C(11)	1.423(9)	C(51)-C(52)	1.358(15)
C(10)-C(25)	1.403(9)	C(52)-H(52)	0.95
C(11)-C(12)	1.389(9)	C(52)-C(53)	1.350(16)
C(11)-C(55)	1.491(9)	C(53)-H(53)	0.95
C(12)-C(13)	1.432(9)	C(53)-C(54)	1.494(15)
C(12)-C(24)	1.439(8)	C(55)-C(56)	1.388(12)
C(13)-H(13)	0.95	C(55)-C(60)	1.331(12)
C(13)-C(14)	1.373(9)	C(56)-C(57)	1.427(13)
C(14)-C(22)	1.444(8)	C(57)-H(57)	0.95
C(15)-C(16)	1.353(9)	C(57)-C(58)	1.366(18)
C(15)-C(20)	1.399(9)	C(58)-H(58)	0.95
C(16)-H(16)	0.95	C(58)-C(59)	1.233(19)
C(16)-C(17)	1.428(10)	C(59)-H(59)	0.95
C(17)-H(17)	0.95	C(59)-C(60)	1.433(13)
C(17)-C(18)	1.395(10)	C(61)-C(62)	1.423(11)
C(18)-C(19)	1.397(10)	C(61)-C(66)	1.347(10)
C(19)-H(19)	0.95	C(62)-C(63)	1.351(11)
C(19)-C(20)	1.355(9)	C(63)-H(63)	0.95
C(20)-C(21)	1.462(9)	C(63)-C(64)	1.337(14)
C(21)-C(22)	1.370(9)	C(64)-H(64)	0.95
C(21)-C(61)	1.468(9)	C(64)-C(65)	1.400(15)
C(22)-C(23)	1.421(9)	C(65)-H(65)	0.95
C(23)-H(23)	0.95	C(65)-C(66)	1.423(12)
C(23)-C(24)	1.378(9)	C(67)-H(67A)	0.98
C(25)-C(26)	1.392(9)	C(67)-H(67B)	0.98
C(26)-H(26)	0.95	C(67)-H(67C)	0.98

5. Additional optoelectronic properties of neutral compounds

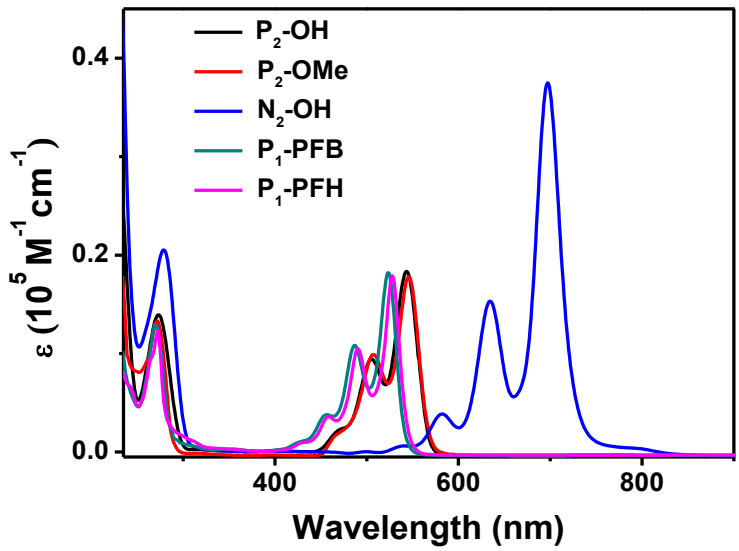

Figure S5. UV-*vis*-NIR absorption spectra of compounds **P2-OH/OMe**, **N2-OH, P1-PFB** and **P1-PFH** recorded in DCM.

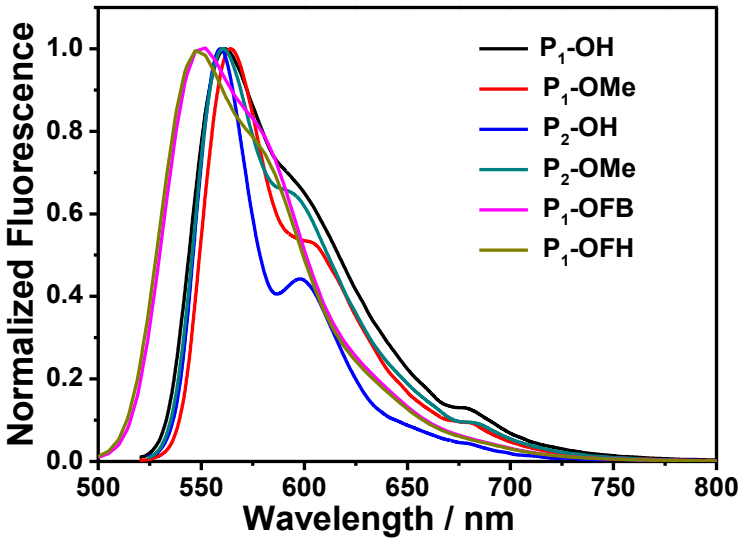

Figure S6. Normalized emission spectra of **P1-OH/OMe** and **P2-OH/OMe** in DCM upon excitation at λ_{exc} = 540 nm and **P1-PFB** and **P1-PFH** in DCM upon excitation at λ_{exc} = 520 nm.

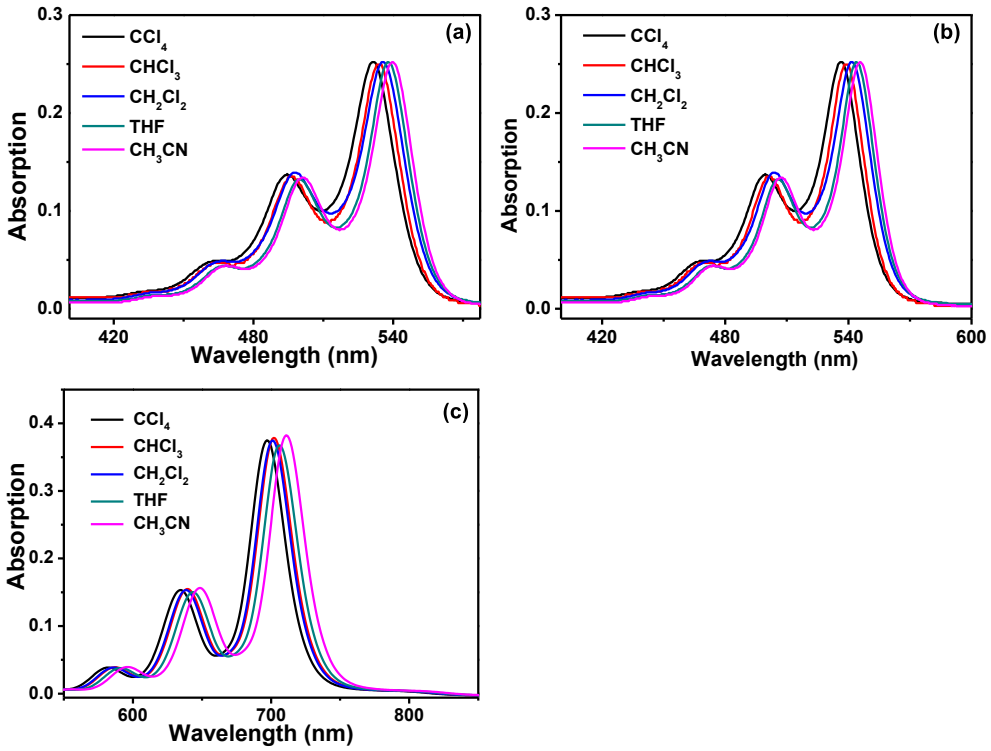

Figure S7. Solvent-dependent absorption spectra of **P1-OH** (a), **P2-OH** (b) and **N1-OH** (c).

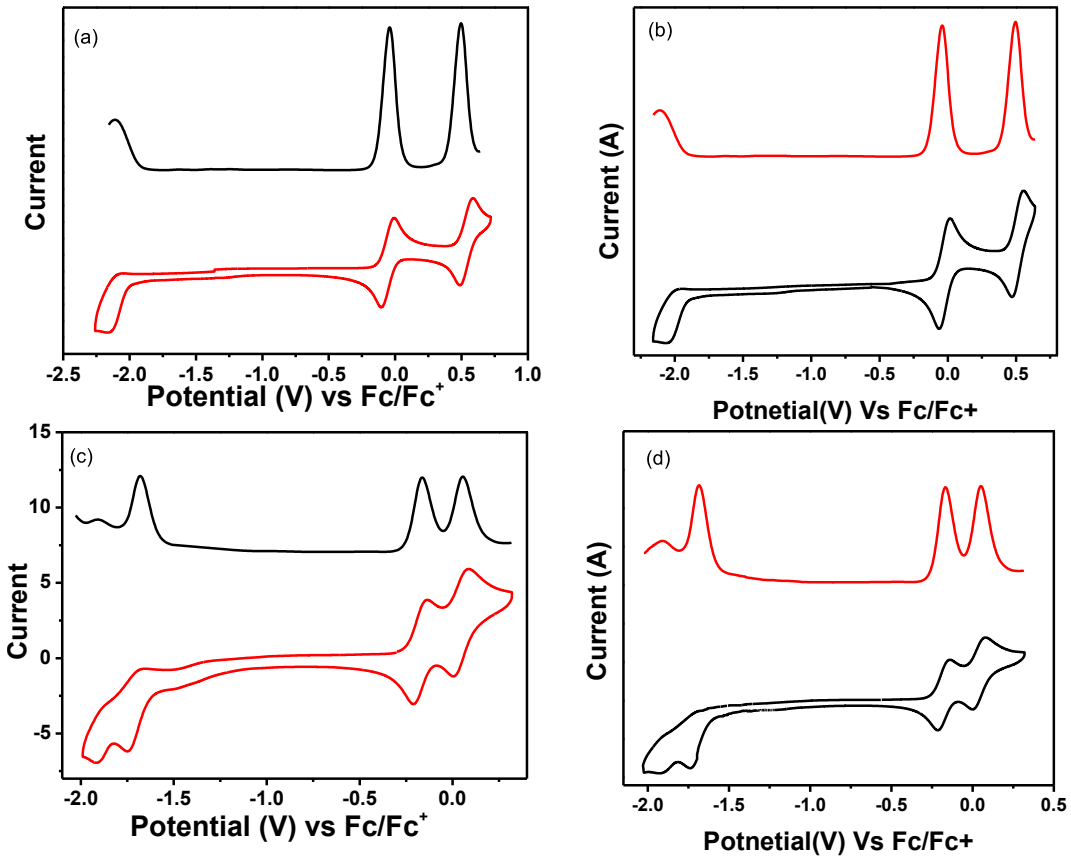

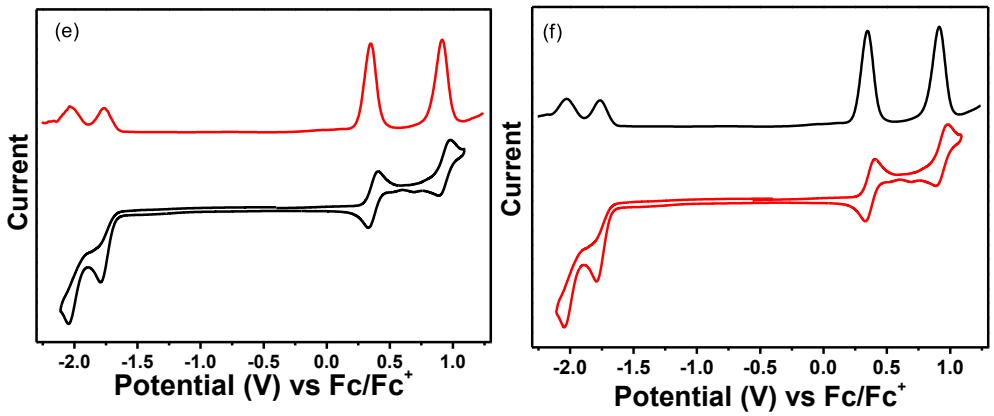

Figure S8. Cyclic voltammogram (black curves) and differential pulse voltammograms (red curves) of **P1-OH** (a), **P2-OH** (b), **N1-OH** (c), **N2-OH** (d), **P1-PFB** (e), and **P1-PFH** (f) solution in DCM (1.0 mM): redox potentials were determined by using 0.10 M *n*-$Bu_4N^+PF_6^-$ as a supporting electrolyte; the electrode potential was externally calibrated by the ferrocene/ferrocenium redox couple.

Table S9. Summary of the photophysical and electrochemical properties of new compounds.

Cmpds	**P1-OH/OMe**	**P2-OH/OMe**	**P1-PFB/PFH**	**N1-OH/OMe**	**N2-OH**
λ_{abs}^{max} (nm)	536/538	544/546	523/528	690/699	696
λ_{em}^{max} (nm)	560/561	559/564	550/548	-	-
E_g^{opt} (eV)[a]	2.14/2.14	2.15/2.18	2.24/2.21	1.45/1.48	1.48
$E_{1/2}^{red1}$ (V)	-/-1.87	-/-1.92	-1.76/-1.77	-1.74/-1.58	-1.70
$E_{1/2}^{red2}$ (V)	-/-	-/-	-2.04/-2.03	-/-1.80	-
$E_{1/2}^{ox1}$ (V)	-0.09/0.03	-0.09/-0.03	0.35/0.36	-0.16/-0.18	-0.17
$E_{1/2}^{ox2}$ (V)	0.43/0.61	0.44/0.58	0.91/0.93	0.06/0.09	0.05
LUMO (eV)[b]	-2.53/-2.83	-2.56/-2.88	-3.13/-3.16	-3.22/-3.15	-3.22
HOMO (eV)[b]	-4.71/-4.81	-4.71/-4.77	-5.11/-5.10	-4.64/-4.62	-4.62
LUMO (eV)[c]	-2.08/-2.01	-2.07/-2.00	-2.46/-2.45	-2.44/-2.40	-2.40
HOMO (eV)[c]	-4.34/-4.26	-4.30/-4.23	-4.79/-4.78	-4.07/-4.03	-4.03

[a]Estimated from absorption onsets; [b]Estimated from onsets of oxidative and reduction waves in CV measurements; [c]Estimated from Gauss calculation.

6. Theoretical calculations of neutral compounds

6.1 DFT and TD-DFT simulations of neutral compounds

DFT and time-dependent DFT (TD-DFT) simulations were performed using the Gaussian 09 software package.[S1] The geometries were optimized at the B3LYP/6-31G (d,p) level, and energies were calculated at the same level of theory. TD-DFT calculations were conducted at PBE/6-31 G(d) level and Um06/6-31 G(d) [S2].

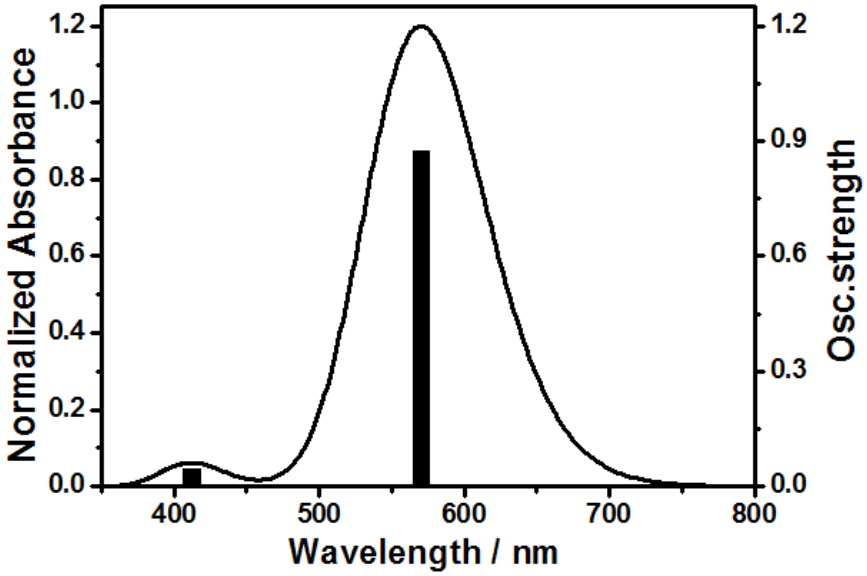

Figure S9. Calculated (PBE/6-31+G*) absorption spectrum of **P_1-OMe**.

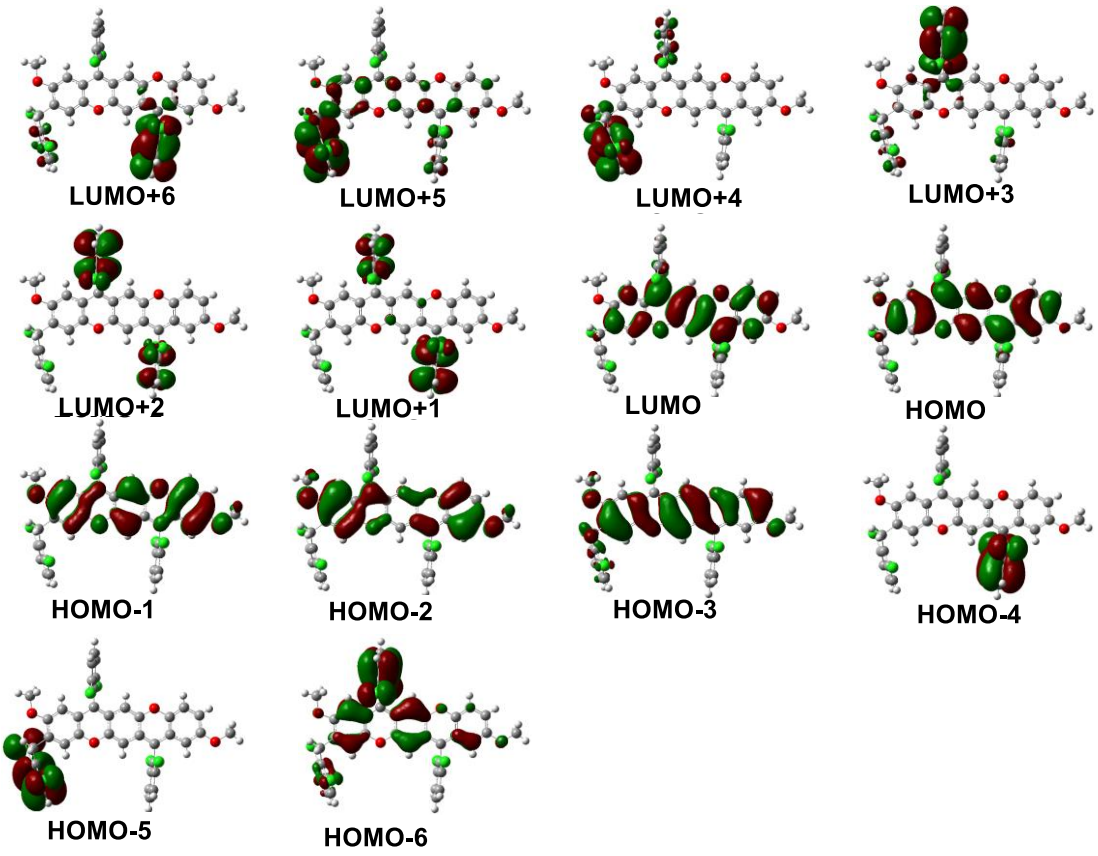

Figure S10. Calculated MOs profiles of **P$_1$-OMe** at the PBE/6-31+G* level.

Table S10. Major electronic transitions of **P$_1$-OMe** calculated by TDDFT method.

excited state	Energy (eV)	Wavelength (nm)	Osc. Strength	Major contribs
1	2.17499	570.11697	0.8759	HOMO->LUMO (99%)
2	2.27251	545.65327	0	HOMO->L+1 (100%)
3	2.31021	536.74764	0	HOMO->L+2 (100%)
4	2.35992	525.44218	7E-4	HOMO->L+3 (99%)
5	2.38702	519.476	0.0045	HOMO->L+4 (100%)
6	2.40592	515.39465	1E-4	HOMO->L+5 (100%)
7	2.43403	509.4438	0.0042	HOMO->L+6 (99%)
8	2.53174	489.78169	6E-4	H-1->LUMO (94%)
9	2.85938	433.6598	4E-4	HOMO->L+7 (87%)
10	3.0088	412.12384	0.0441	H-2->LUMO (93%)
11	3.06831	404.13096	0	HOMO->L+8 (100%)

12	3.13152	395.97374	3E-4	HOMO->L+9 (100%)
13	3.14132	394.73825	0.0013	HOMO->L+10 (100%)
14	3.26474	379.816	0	H-1->L+1 (100%)
15	3.30234	375.49089	0	H-1->L+2 (100%)

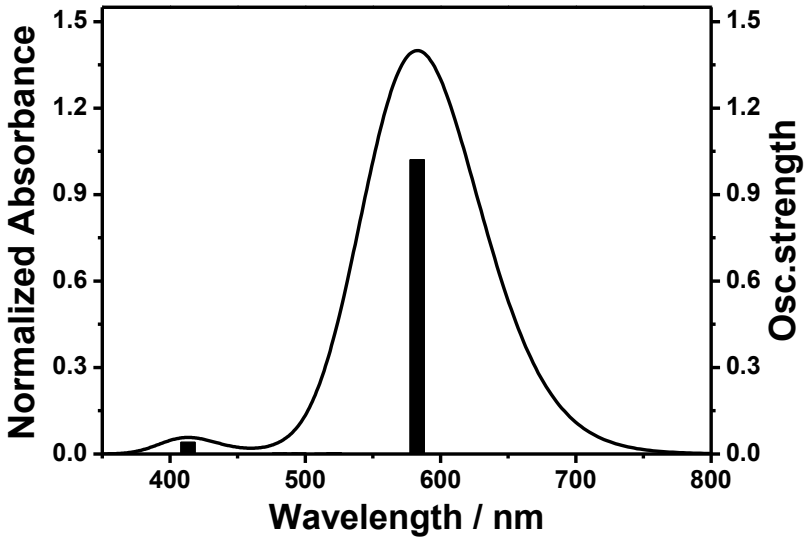

Figure S11. Calculated (PBE/6-31 G*) absorption spectrum of **P_2-OMe**.

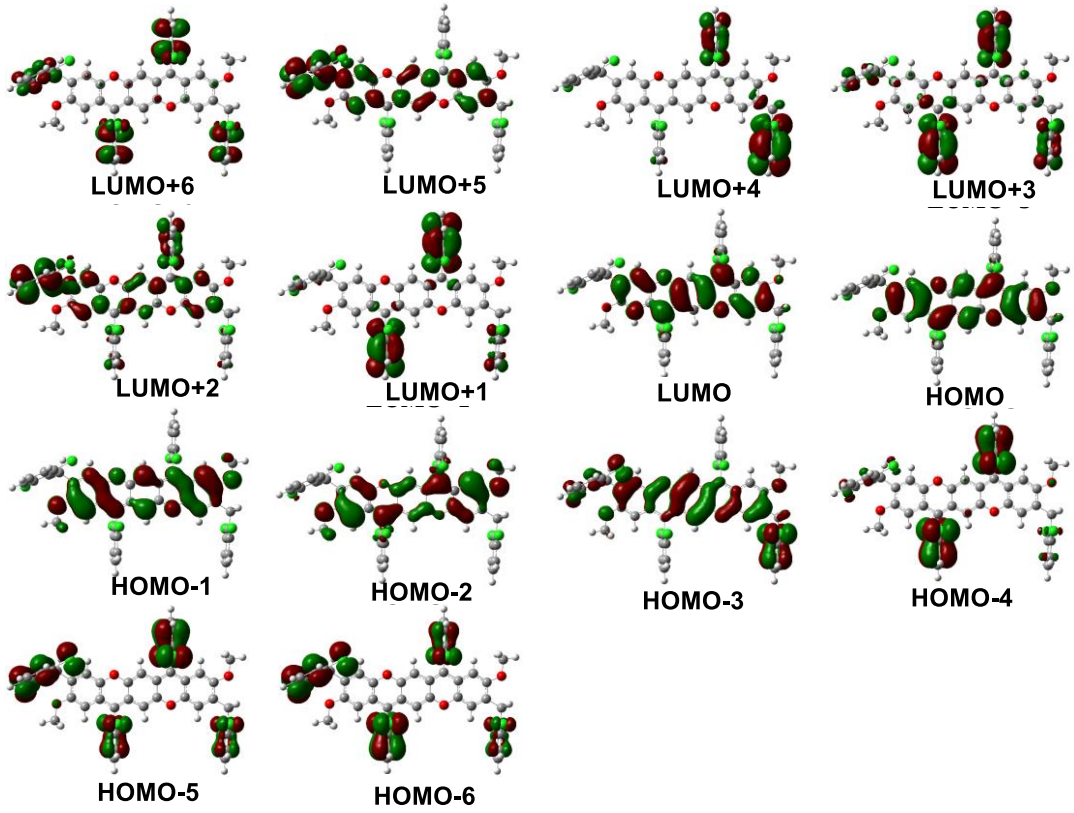

Figure S12. Calculated MOs profiles of **P_2-OMe** at the PBE/6-31+G* level.

Table S11. Major electronic transitions of **P_2-OMe** calculated by TDDFT method.

excited state	Energy (eV)	Wavelength (nm)	Osc. Strength	Major contribs
1	2.12789	582.738	1.0215	HOMO->LUMO (98%)
2	2.2648	547.50866	0.0016	HOMO->L+1 (100%)
3	2.30091	538.9174	1E-4	HOMO->L+2 (100%)
4	2.35152	527.3194	0	HOMO->L+3 (99%)
5	2.37842	521.3546	0.0042	HOMO->L+4 (100%)
6	2.39362	518.04344	1E-4	HOMO->L+5 (100%)
7	2.42143	512.09507	0.0027	HOMO->L+6 (99%)
8	2.50354	495.29936	0.0033	H-1->LUMO (36%), HOMO->L+7 (61%)
9	2.53624	488.91256	0.0024	H-1->LUMO (52%), HOMO->L+7 (23%), HOMO->L+8 (21%)
10	2.57825	480.94704	0.0033	HOMO->L+7 (12%), HOMO->L+8 (76%)
11	2.84038	436.56104	0	HOMO->L+9 (86%)
12	2.9998	413.36046	0.0409	H-2->LUMO (90%)
13	3.05571	405.79759	0	HOMO->L+10 (100%)
14	3.12492	396.81017	2E-4	HOMO->L+11 (100%)
15	3.13272	395.82204	0.0012	HOMO->L+12 (100%)

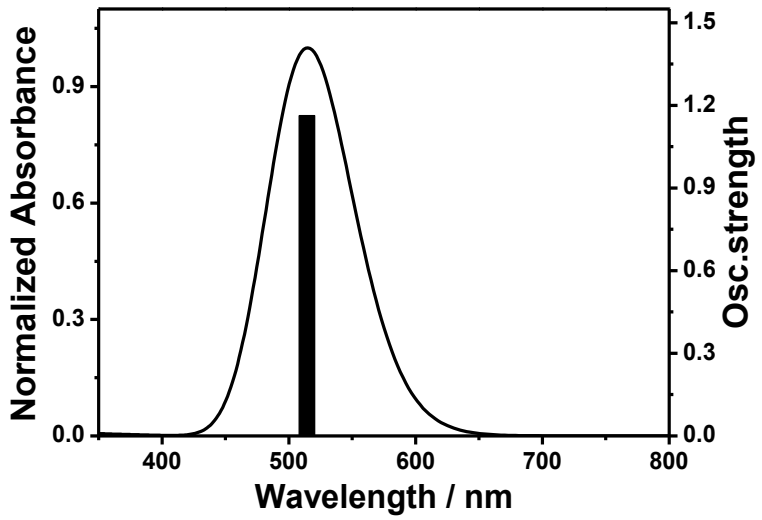

Figure S13. Calculated (B3LYP/6-31 G*) absorption spectrum of **P_1-PFB**.

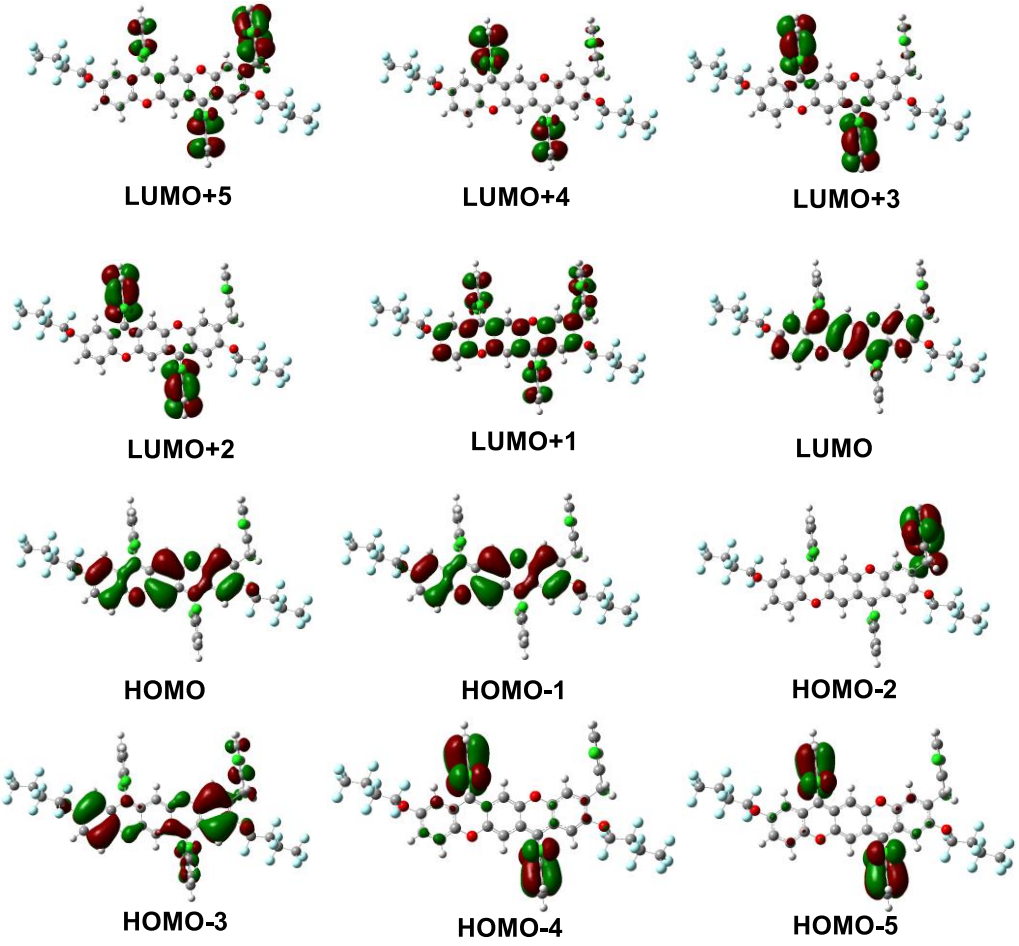

Figure S14. Calculated MOs profiles of **P_1-PFB** at the B3LYP/6-31 G* level.

Table S12. Major electronic transitions of **P_1-PFB** calculated by TDDFT method.

excited state	Energy (cm^{-1})	Wavelength (nm)	Osc. Strength	Major contribs

1	19446.02728	514.2438532	1.1634	HOMO->LUMO (100%)
2	25217.73078	396.5463859	0.0005	H-1->LUMO (11%), HOMO->L+1 (82%)
3	25798.44997	387.620187	0.0002	H-1->LUMO (83%), HOMO->L+1 (11%)
4	25811.35484	387.426389	0.0005	HOMO->L+2 (95%)
5	26135.58972	382.6200253	0	HOMO->L+3 (98%)
6	27229.27752	367.2517566	0.0026	HOMO->L+4 (97%)
7	27555.12551	362.9088895	0.0003	HOMO->L+5 (60%), HOMO->L+6 (19%), HOMO->L+7 (16%)
8	28948.85157	345.4368467	0.0012	HOMO->L+5 (33%), HOMO->L+6 (57%)
9	29358.58122	340.6159149	0.0037	HOMO->L+6 (22%), HOMO->L+7 (69%)
10	31089.44702	321.6525528	0.0006	HOMO->L+8 (82%)
11	31231.4006	320.1905713	0.008	H-3->LUMO (38%), HOMO->L+9 (54%)
12	32231.52809	310.255225	0.0004	H-5->LUMO (41%), H-4->LUMO (48%)
13	32250.8854	310.0690067	0.0003	H-5->LUMO (52%), H-4->LUMO (44%)
14	33108.25276	302.0394967	0.0794	H-3->LUMO (47%), HOMO->L+9 (41%)
15	33335.70111	299.9786916	0.0009	H-2->LUMO (98%)

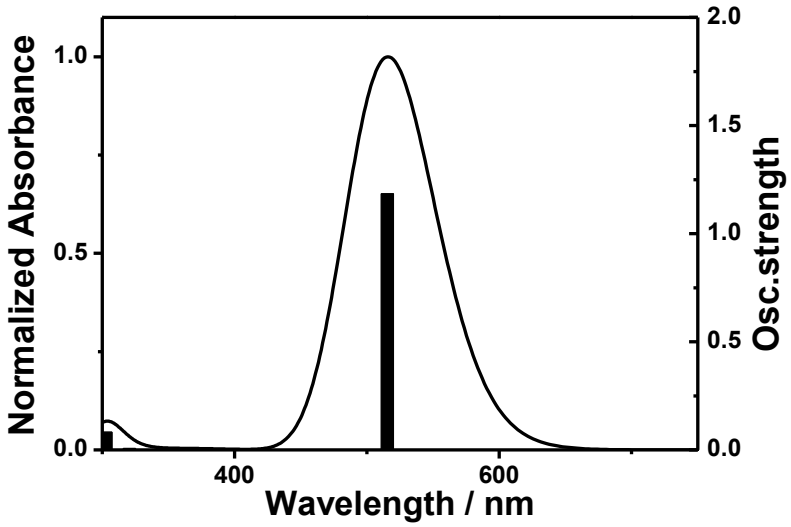

Figure S15. Calculated (B3LYP/6-31 G*) absorption spectrum of **P_1-PFH.**

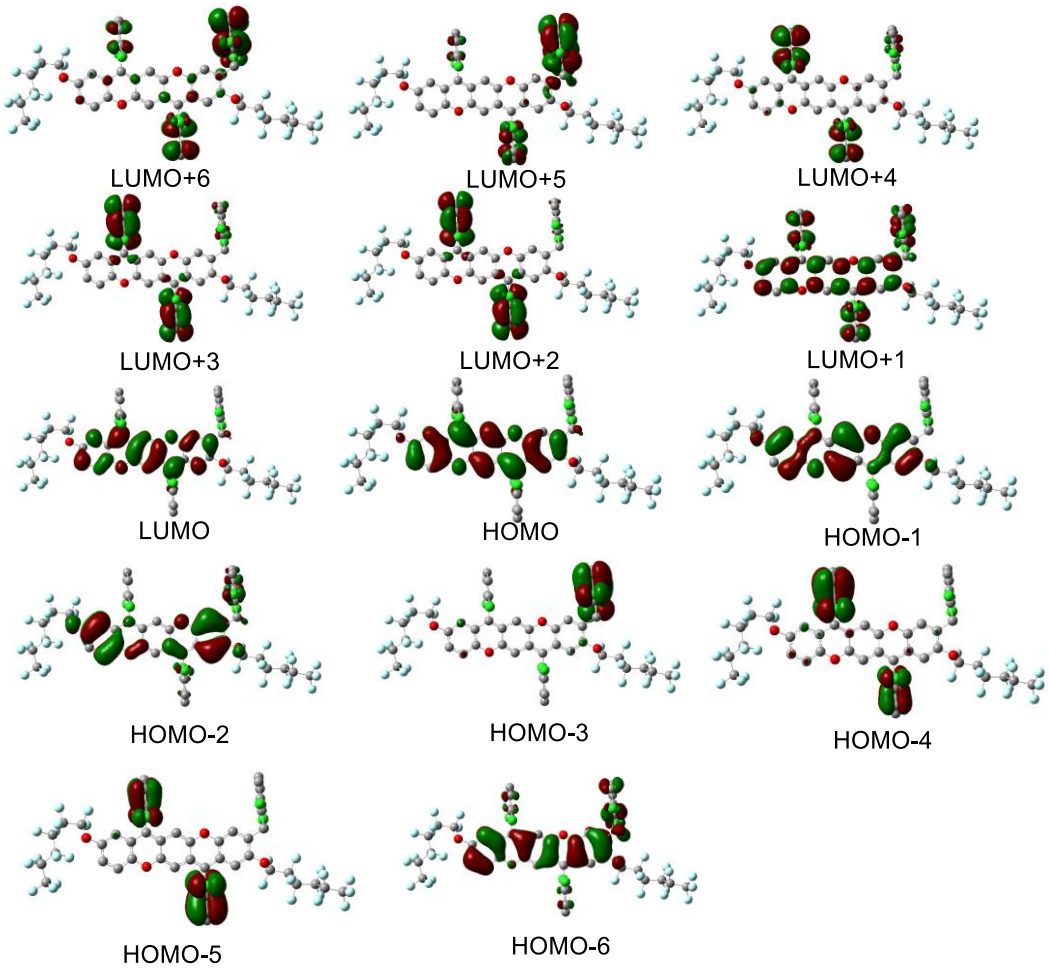

Figure S16. Calculated MOs profiles of **P_1-PFH** at the B3LYP/6-31 G* level.

Table S13. Major electronic transitions of **P_1-PFH** calculated by TDDFT method.

excited state	Energy (cm^{-1})	Wavelength (nm)	Osc. Strength	Major contribs
1	19404.08645	515.3553621	1.1847	HOMO->LUMO (100%)
2	25180.62927	397.1306631	0.0006	H-1->LUMO (13%), HOMO->L+1 (80%)
3	25718.60108	388.8236366	0.0003	HOMO->L+2 (98%)
4	25758.12224	388.2270573	0.0006	H-1->LUMO (84%), HOMO->L+1 (12%)
5	26042.0294	383.9946513	0	HOMO->L+3 (97%)
6	27134.91065	368.5289451	0.0025	HOMO->L+4 (97%)

7	27481.72906	363.8781235	0.0002	HOMO->L+5 (19%), HOMO->L+6 (47%), HOMO->L+7 (28%)
8	28697.20658	348.4659725	0.0005	HOMO->L+5 (78%), HOMO->L+6 (15%)
9	29108.54934	343.5416819	0.0026	HOMO->L+6 (34%), HOMO->L+7 (59%)
10	31095.0929	321.5941509	0.0015	H-2->LUMO (17%), HOMO->L+8 (64%)
11	31194.2991	320.5713957	0.0067	H-2->LUMO (25%), HOMO->L+8 (19%), HOMO->L+9 (43%)
12	32298.47211	309.6121688	0.0001	H-4->LUMO (90%)
13	32310.57043	309.4962382	0.0006	H-5->LUMO (90%)
14	33030.82353	302.7475228	0.0829	H-2->LUMO (46%), HOMO->L+9 (43%)
15	33526.04795	298.2755383	0.0002	H-3->LUMO (96%)

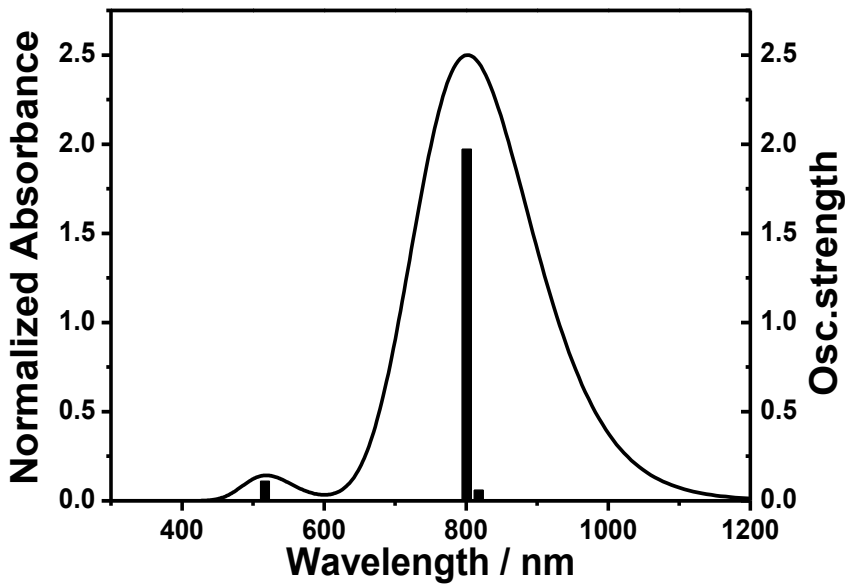

Figure S17. Calculated (PBE/6-31 G*) absorption spectrum of **N_1-OH.**

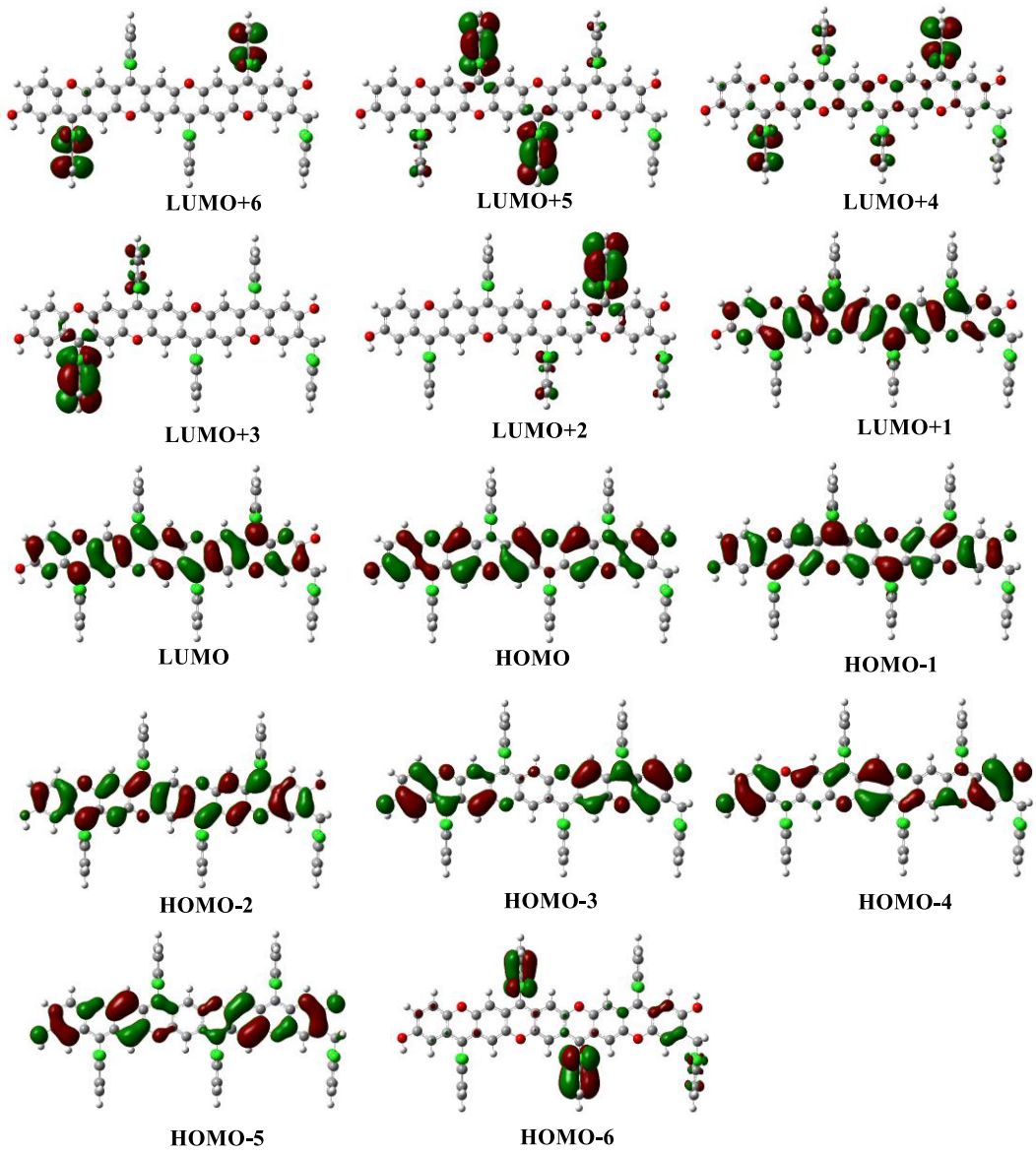

Figure S18. Calculated MOs profiles of **N_1-OH** at the PBE/6-31+G* level.

Table S14. Major electronic transitions of **N_1-OH** calculated by TDDFT method.

excited state	Energy (eV)	Wavelength (nm)	Osc. Strength	Major contribs
1	1.5164	817.7241567	0.0596	H-1->LUMO (46%), HOMO->L+1 (51%), HOMO->LUMO (3%)
2	1.54831	800.8742112	1.9717	HOMO->LUMO (100%)
3	2.11888	585.2135214	0.0002	HOMO->L+2 (100%)

4	2.12739	582.8749783	0.0001	HOMO->L+3 (100%)
5	2.17049	571.2991275	0.0047	H-2->LUMO (95%)
6	2.1982	564.0990793	0.0013	HOMO->L+4 (94%)
7	2.1997	563.7143614	0	HOMO->L+5 (99%)
8	2.2143	559.9970038	0.0001	HOMO->L+6 (98%)
9	2.2382	554.016429	0.0001	HOMO->L+7 (100%)
10	2.27421	545.2453346	0	HOMO->L+9(98%)
11	2.27731	544.5030155	0.0001	HOMO->L+8(94%)
12	2.30451	538.0754129	0.0012	HOMO->L+10 (95%)
13	2.31051	536.6779354	0.0003	HOMO->L+11 (97%)
14	2.35302	526.9831965	0.0017	H-3->LUMO (50%), H-1->LUMO (24%), HOMO->L+1 (20%)
15	2.39992	516.6833499	0.1106	H-1->L+1 (62%), HOMO->L+12 (31%)

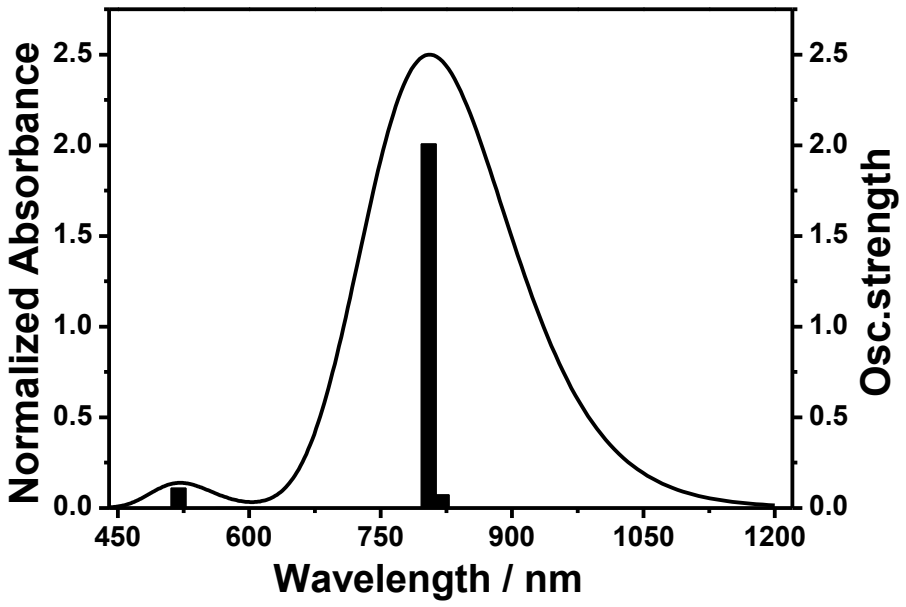

Figure S19. Calculated (PBE/6-31 G*) absorption spectrum of **N_1-OMe**.

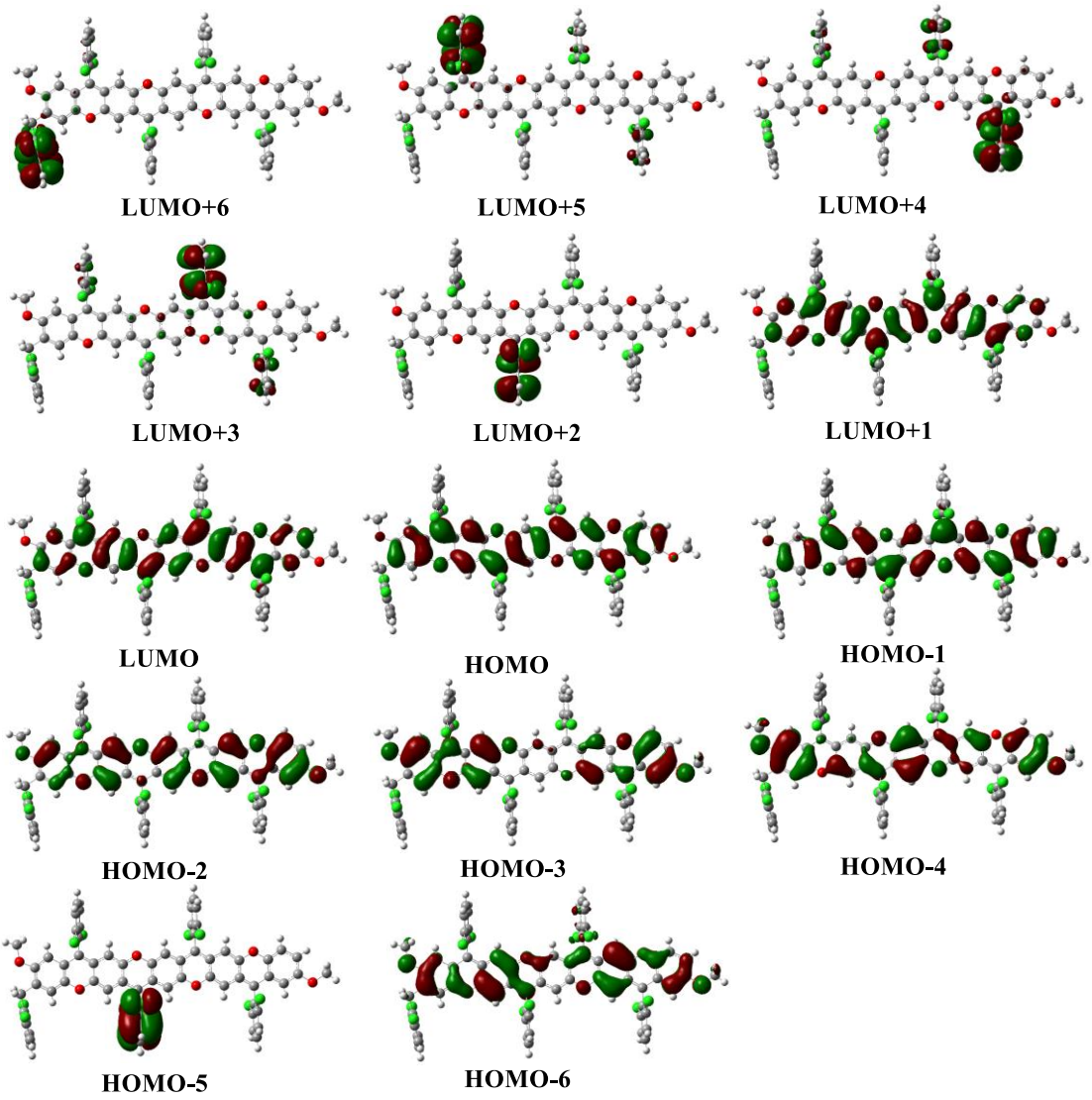

Figure S20. Calculated MOs profiles of **N_1-OMe** at the PBE/6-31+G* level.

Table S15. Major electronic transitions of **N_1-OMe** calculated by TDDFT method.

excited state	Energy (eV)	Wavelength (nm)	Osc. Strength	Major contribs
1	1.5131	819.5078	0.0726	H-1->LUMO (46%), HOMO->L+1 (51%) HOMO->LUMO (4%)
2	1.54041	804.9821	2.0072	HOMO->LUMO (100%)
3	2.10068	590.2844	0	HOMO->L+2 (100%)
4	2.11058	587.5152	0	HOMO->L+3 (100%)
5	2.17509	570.0908	0.0033	H-2->LUMO (24%),

				HOMO->L+4 (74%)
6	2.17879	569.1225	0	HOMO->L+5 (100%)
7	2.18509	567.4814	0.0024	H-2->LUMO (72%), HOMO->L+4 (22%)
8	2.19509	564.8958	$1.00E^{-4}$	HOMO->L+6 (98%)
9	2.2168	559.3654	0	HOMO->L+7 (100%)
10	2.2384	553.9669	0	HOMO->L+8 (100%)
11	2.2548	549.9372	0	HOMO->L+9 (95%)
12	2.2694	546.3987	0.0017	HOMO->L+10 (97%)
13	2.28771	542.0274	0	HOMO->L+11 (99%)
14	2.35052	527.5438	0.002	H-3->LUMO (41%), H-1->LUMO (30%), HOMO->L+1 (25%)
15	2.38812	519.2367	0.1098	H-1->L+1 (60%), HOMO->L+12 (34%)

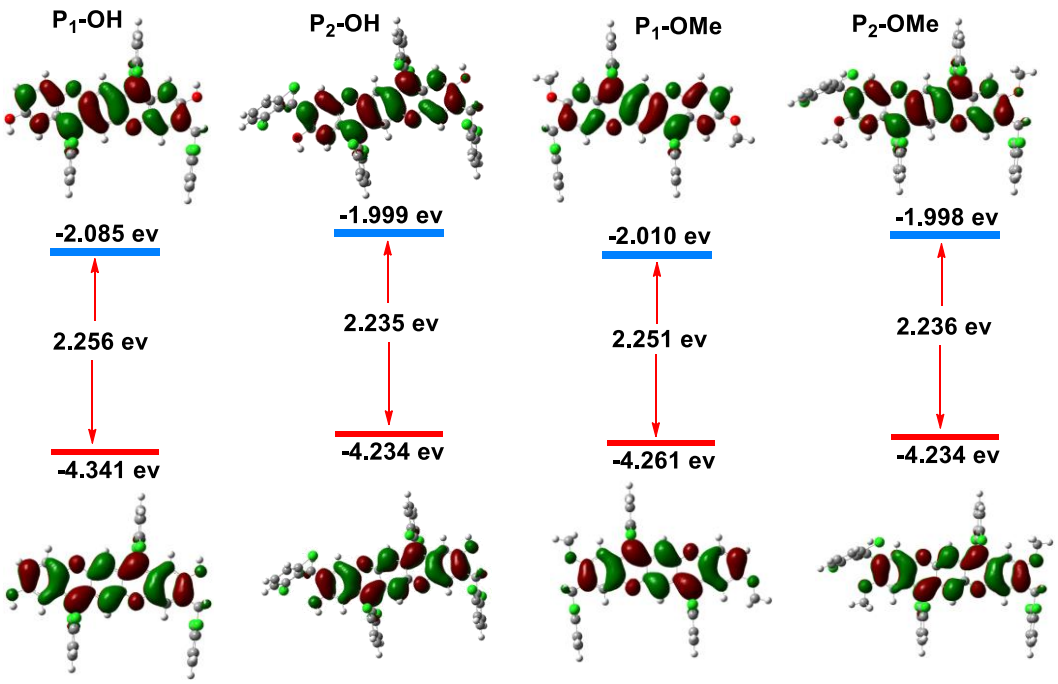

Figure S21. LUMOs (top) and HOMOs (bottom) of O-pentacenes (**P_1-OH**, **P_2-OH**, **P_1-OMe** and **P_2-OMe**) and their energy band gaps obtained from DFT calculations at the B3LYP/6-31G (d,p) level.

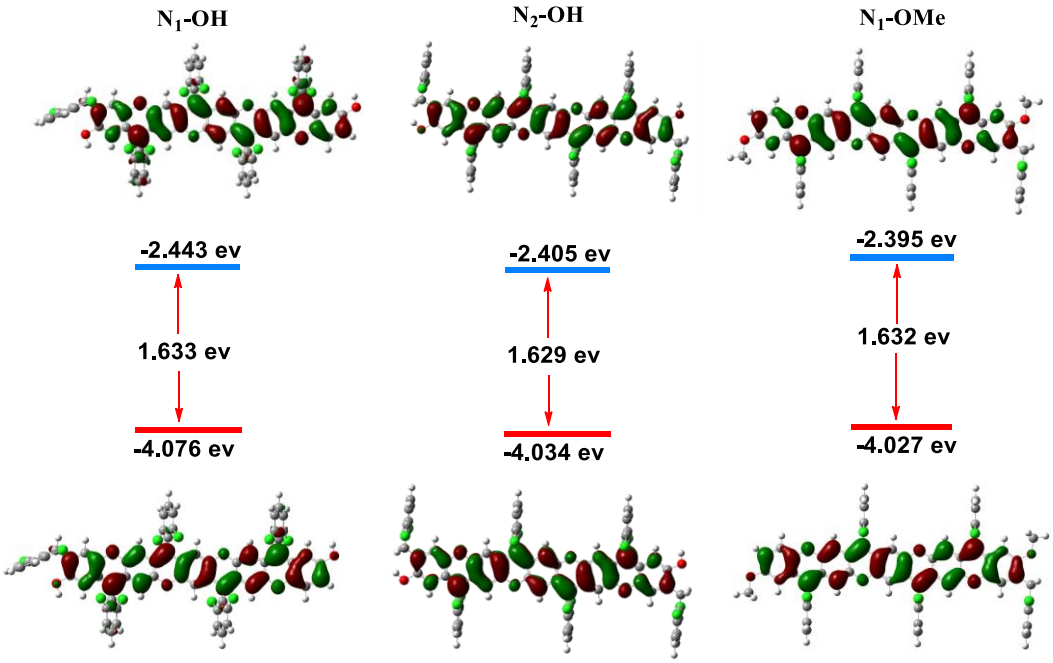

Figure S22. LUMOs (top) and HOMOs (bottom) of O-nonacenes (**N_1-OH**, **N_2-OH** and **N_1-OMe**) and their energy gaps obtained from DFT calculations at the B3LYP/6-31G(d,p) level.

7. Characterization of positively charged O-pentacene and O-nonacene

7.1 UV-*vis*-NIR spectroscopic characterization of cationic radical

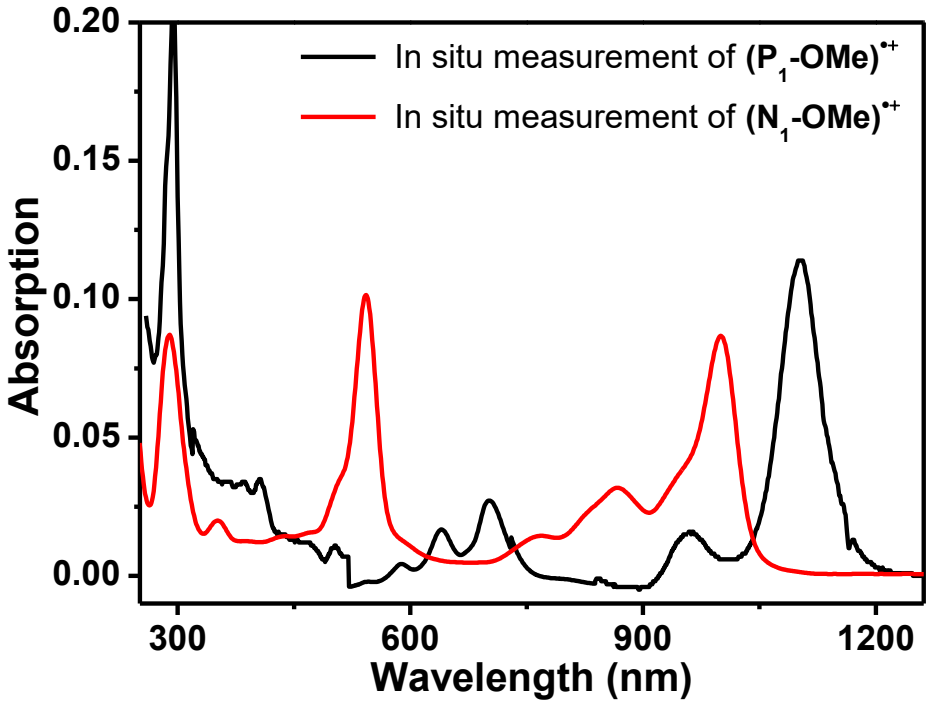

Figure S23. UV-*vis*-NIR spectrum of **(P$_1$-OMe)$^{\bullet+}$** and **(N$_1$-OMe)$^{\bullet+}$** via in situ measurement of one-electron oxidation of **P$_1$-OMe** and **N$_1$-OMe** by the electrochemical method (DCM solution containing 0.1 M *n*-Bu$_4$NPF$_6$).

7.2 TD-DFT simulations of positively charged species

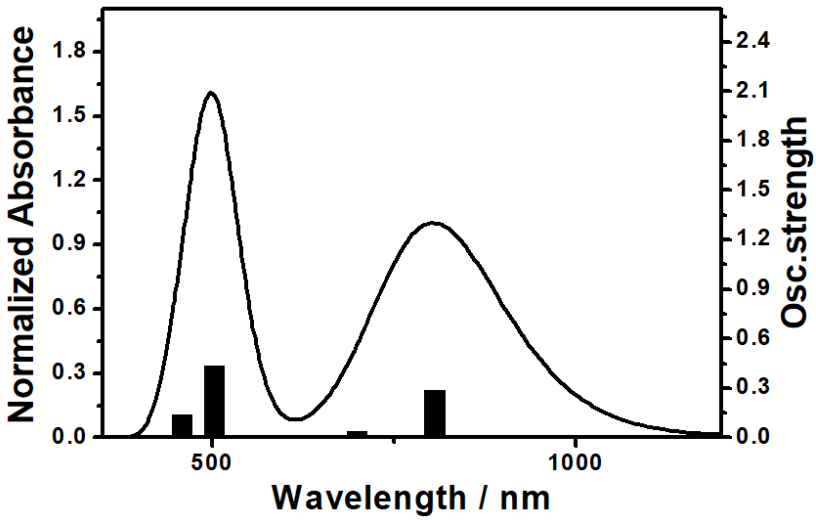

Figure S24. Calculated (UM06/6-31+G*) absorption spectrum of **(P$_1$-OMe)$^{\bullet+}$•SbF$_6^-$**.

Table S16. Major electronic transitions of **(P$_1$-OMe)$^{\bullet+}$•SbF$_6^-$** calculated by TDDFT method.

excited state	Energy (cm^{-1})	Wavelength (nm)	Osc. Strength	Major contribs
1	10849.03856	921.7406634	0.015	HOMO(A)->LUMO(A) (16%), HOMO(B)->LUMO(B) (81%)
2	12405.69936	806.0811172	0.2883	HOMO(A)->LUMO(A) (72%), HOMO(B)->LUMO(B) (13%)
3	14297.88912	699.4039411	0.0388	H-1(A)->LUMO(A) (10%), H-2(B)->LUMO(B) (77%)
4	15953.7568	626.8116109	0.0018	H-1(B)->LUMO(B) (99%)
5	18059.68496	553.7195152	0.0001	H-3(B)->LUMO(B) (99%)
6	18465.38464	541.5538422	0.0015	H-4(B)->LUMO(B) (99%)
7	19041.26848	525.1750959	0.0012	H-1(A)->LUMO(A) (66%), H-2(B)->LUMO(B) (15%), HOMO(B)->L+1(B) (12%)
8	19361.4728	516.489634	0.0114	H-5(B)->LUMO(B) (98%)
9	19872.83184	503.199548	0.4333	H-6(B)->LUMO(B) (82%)
10	21068.15376	474.6500388	0	H-7(B)->LUMO(B) (98%)
11	21773.0872	459.2825954	0.1355	H-4(A)->LUMO(A) (42%), H-9(B)->LUMO(B) (31%), H-2(B)->L+1(B) (10%)
15	22878.0744	437.0997237	0.0007	H-1(A)->LUMO(A) (13%), HOMO(B)->L+1(B) (59%)

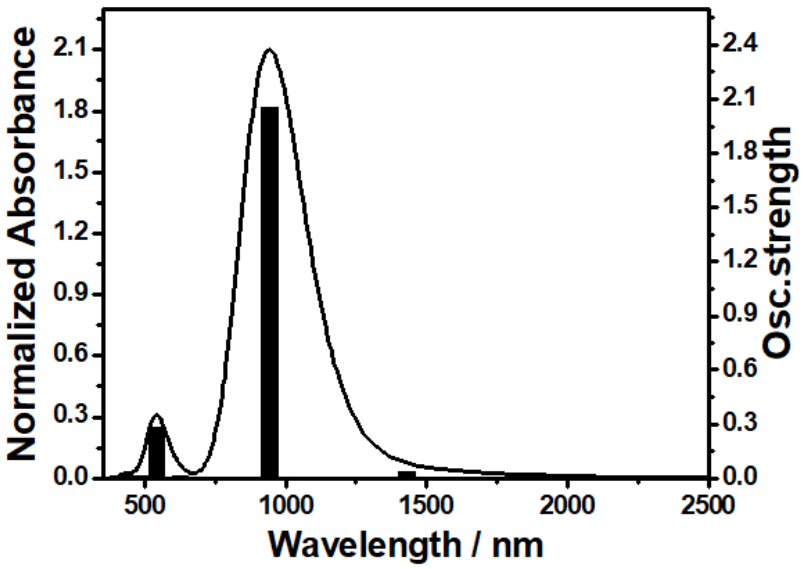

Figure S25. Calculated (UM06/6-31+G*) absorption spectrum of **$(N_1\text{-OMe})^{\bullet+}\bullet SbF_6^-$**.

Table S17. Major electronic transitions of **$(N_1\text{-OMe})^{\bullet+}\bullet SbF_6^-$** calculated by TDDFT method.

excited state	Energy (cm^{-1})	Wavelength (nm)	Osc. Strength	Major contribs
1	6991.26208	1430.356906	0.0383	HOMO(A)->LUMO(A) (59%), HOMO(B)->LUMO(B) (40%)
2	10627.23456	940.9785719	2.0576	HOMO(A)->LUMO(A) (30%), HOMO(B)->LUMO(B) (53%)
3	11619.30336	860.6367947	0.0078	H-1(A)->LUMO(A) (41%), HOMO(A)->L+1(A) (21%), HOMO(B)->L+1(B) (33%)
4	14510.0144	689.179192	0.0018	H-1(B)->LUMO(B) (82%)
5	15988.43888	625.4519328	0.0116	H-2(B)->LUMO(B) (73%)
6	16271.54144	614.5699249	0.0048	H-1(A)->LUMO(A) (39%), HOMO(A)->L+1(A) (56%)
7	18480.70928	541.104773	0.2815	H-1(A)->L+1(A) (30%), HOMO(B)->L+2(B) (34%)
8	18817.0448	531.433076	0.0115	H-4(B)->LUMO(B) (53%)

9	19423.57792	514.8382055	0.0006	H-1(A)->LUMO(A) (12%), HOMO(A)->L+1(A) (11%), HOMO(B)->L+1(B) (50%)
10	19642.15568	509.1090898	0.0114	H-2(A)->LUMO(A) (56%), H-2(B)->LUMO(B) (10%)
11	21356.90224	468.2327	0	H-3(A)->LUMO(A) (41%), H-4(B)->LUMO(B) (16%)
12	21857.776	457.5030872	0	H-3(B)->LUMO(B) (94%)
13	22295.73808	448.5162126	0.0113	H-5(A)->LUMO(A) (18%), HOMO(A)->L+2(A) (20%), H-10(B)->LUMO(B) (16%)
14	23139.39984	432.1633262	0.0033	HOMO(A)->L+2(A) (12%), H-6(B)->LUMO(B) (62%)
15	23305.5512	429.082321	0.0115	H-2(A)->LUMO(A) (12%), H-6(B)->LUMO(B) (12%), H-1(B)->L+1(B) (43%)

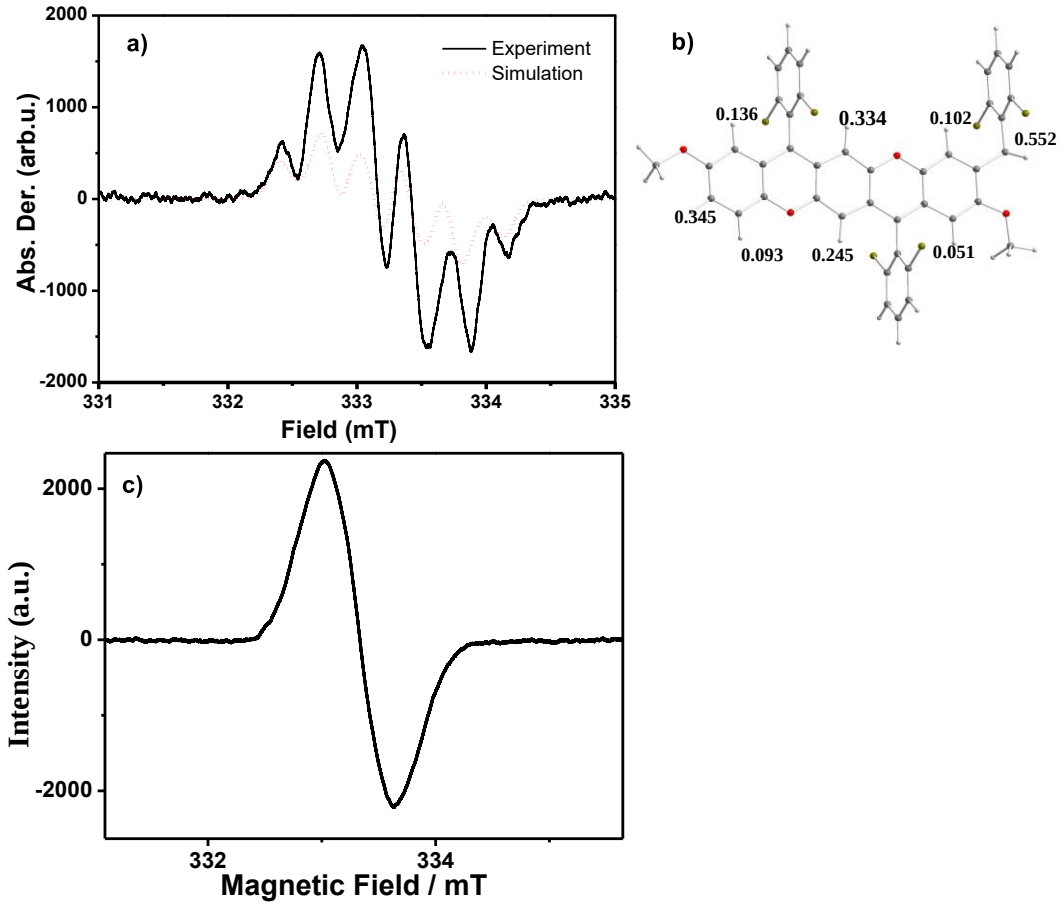

Figure S26. (a) ESR spectra of **(P$_1$-OMe)$^{\bullet+}$•SbF$_6^-$** (g_e = 2.0032) and simulated one with the coupling constants (b), and (c) **(N$_1$-OMe)$^{\bullet+}$•SbF$_6^-$** (g_e = 2.0029) recorded in degassed DCM solution at room temperature.

7.3 Spin density of radical cation

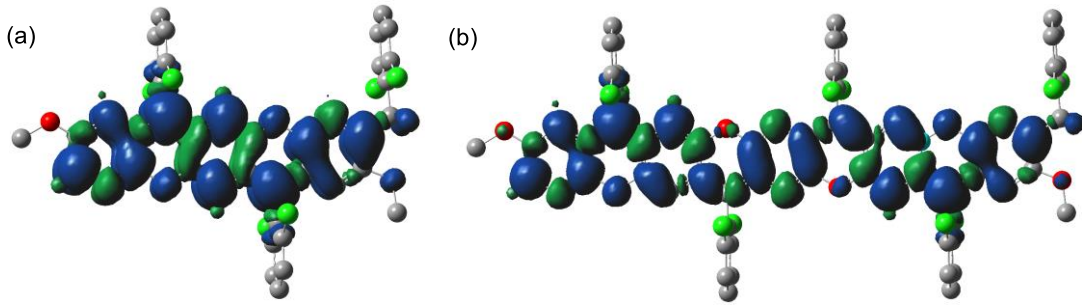

Figure S27. Spin density maps of **(P$_1$-OMe)$^{\bullet+}$•SbF$_6^-$** (a) and **(N$_1$-OMe)$^{\bullet+}$•SbF$_6^-$** (b). Hydrogen atoms are omitted for clarity.

7.4 Calculated aromaticity of radical cation.

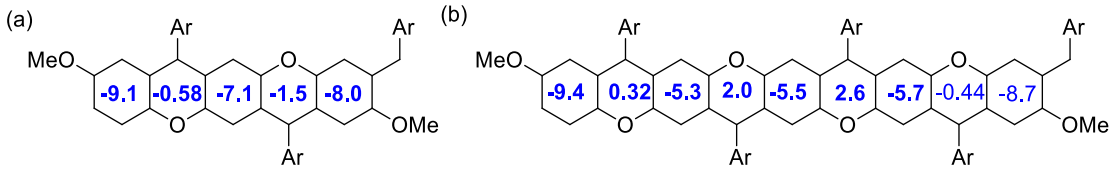

Figure S28. NICS values of π-framework **(P1-OMe)**$^{\bullet+}$ (a) and **(N1-OMe)**$^{\bullet+}$ (b), obtained from DFT calculations at the GIAO-B3LYP/6-311+G(d, p) level.

7.5 Dications of P1-OMe and N1-OMe

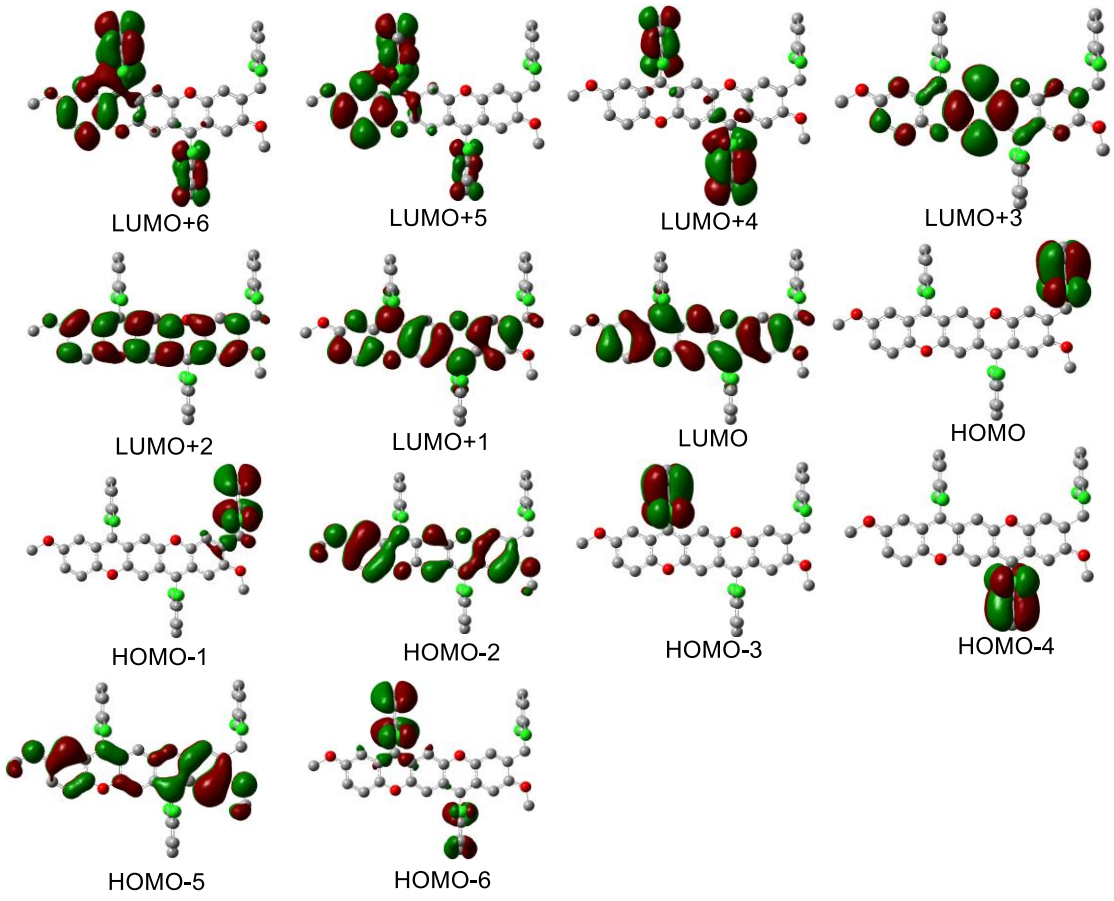

Figure S29. Calculated MOs profiles of **(P1-OMe)**$^{2+}$ at the M06/6-31+G* level.

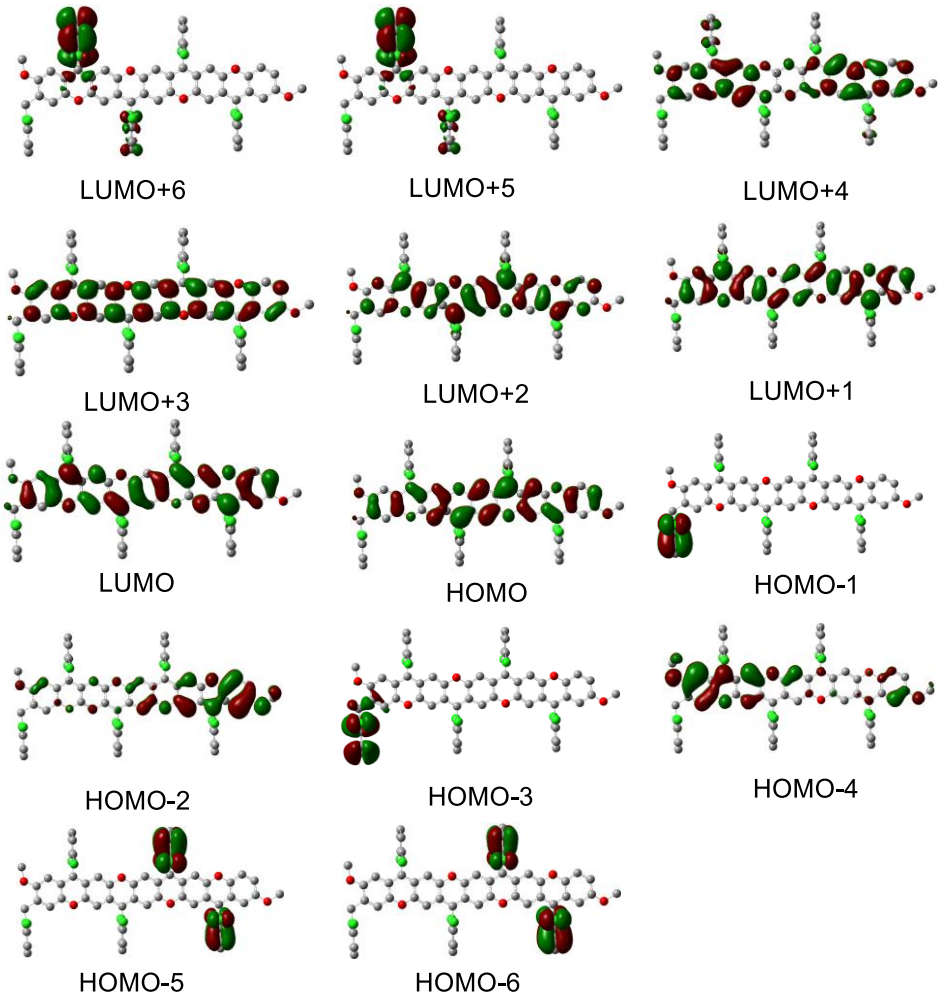

Figure S30. Calculated MOs profiles of **$(N_1\text{-OMe})^{2+}$** at the M06/6-31+G* level.

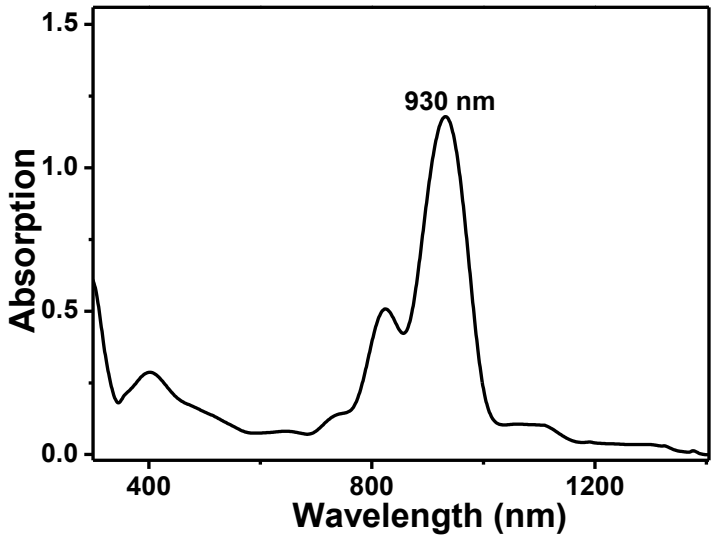

Figure S31. UV-*vis*-NIR absorption spectrum of **$(N_1\text{-OMe})^{2+}$** recorded in DCM.

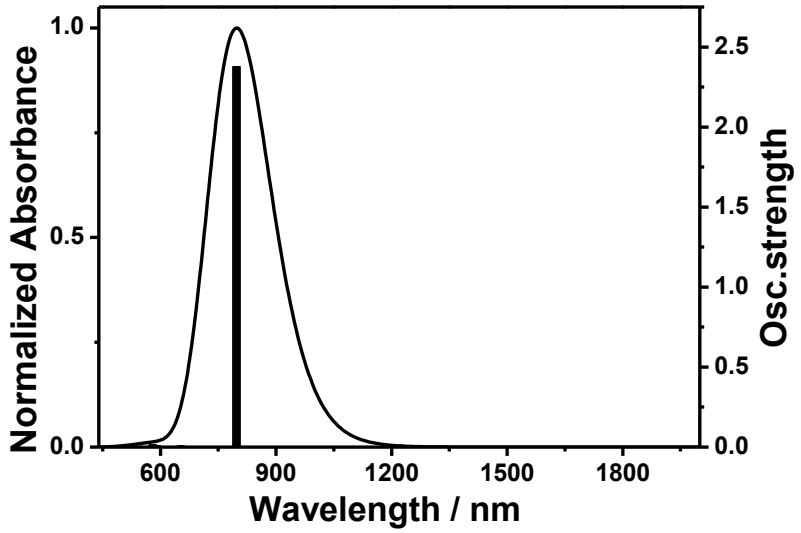

Figure S32. Calculated (M06/6-31+G*) absorption spectrum of **$(N_1\text{-OMe})^{2+}$**.

Table S18. Major electronic transitions of **$(N_1\text{-OMe})^{2+}$** calculated by TDDFT method.

excited state	Energy (cm^{-1})	Wavelength (nm)	Osc. Strength	Major contribs
1	12543.53448	797.2234633	2.3776	HOMO->LUMO (102%)
2	14029.20774	712.798626	0.0031	H-1->LUMO (97%)
3	15325.34071	652.5140414	0.0077	H-2->LUMO (93%)
4	16471.45455	607.1109246	0	H-3->LUMO (95%)
5	16955.38721	589.7830511	0.0096	H-4->LUMO (37%), HOMO->L+1 (57%)
6	17248.97302	579.7446601	0.014	H-4->LUMO (53%), HOMO->L+1 (33%)
7	18308.78554	546.1858723	0	H-6->LUMO (92%)
8	18378.95577	544.100553	0.0002	H-5->LUMO (98%)
9	18571.72228	538.4530227	0	H-7->LUMO (98%)
10	19378.27671	516.041759	0.0002	H-8->LUMO (88%)
11	19519.42374	512.3102062	0.0058	H-9->LUMO (78%)
12	20836.52712	479.9264265	0.0001	H-1->L+1 (95%)

8. OFET devices

8.1 Thin film deposition and device fabrication

Bottom-gate/bottom-contact OFET devices were fabricated by using Si/SiO_2 substrates where Si and SiO_2 were worked as the gate electrode and the gate dielectric, respectively. The source and drain gold electrodes with thickness of 50 nm using 2 nm of chromium as an adhesion layer were formed by standard lithography procedures. Prior to deposition, the wafers were cleaned up with ultrapure water, acetone, isopropanol, and then treated by oxygen plasma and passivated by trichloro(octadecyl)silane to reduce the traps. Finally, the films were deposited by spin-coating at 1500 rpm. The length and width of channel were 80 μm and 1000 μm, respectively.

8.2 The parameters of charge carrier mobilities

The charge carrier mobilities of OFETs were calculated in the saturation regime from a plot of the square root of the drain current vs. gate voltage using the following equation:

$$I_{\mathrm{DS}} = \frac{WC_i}{2L}\mu(V_G - V_T)^2$$

where I_{DS} is the drain-source current, C_i is the capacitance per unit area of the gate dielectric(10 nF/cm^2), L is the channel length, W is the channel width, V_G and V_T are the gate-source voltage and threshold voltage,respectively.

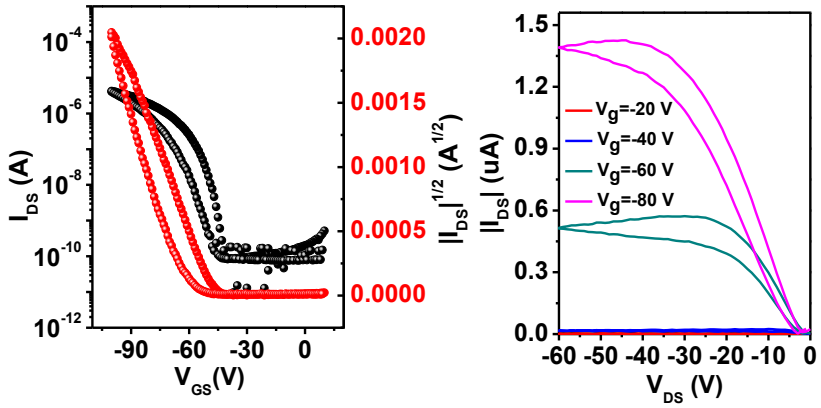

Figure S33. Transfer (left) and output (right) characteristics of **P1-PFB** thin-film based bottom-contact bottom-gate OFET (I_{DS} = source-drain current, and V_{GS} = gate voltage, V_{DS} = source-drain voltage).

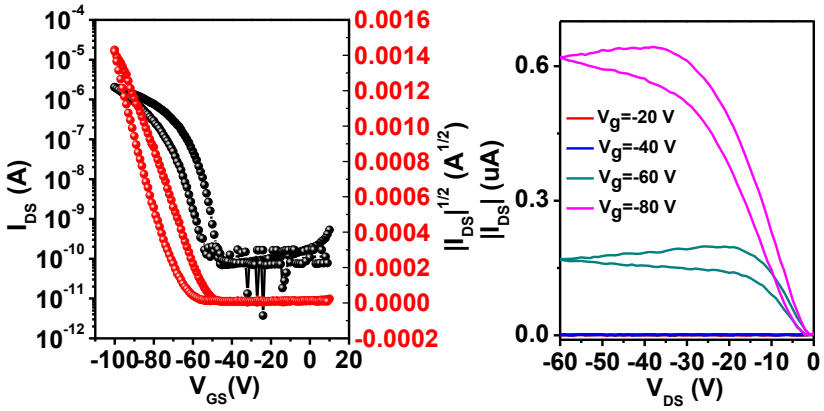

Figure S34. Transfer (left) and output (right) characteristics of **P1-PFH** thin-film based bottom-contact bottom-gate OFET (I_{DS} = source-drain current, and V_{GS} = gate voltage, V_{DS} = source-drain voltage).

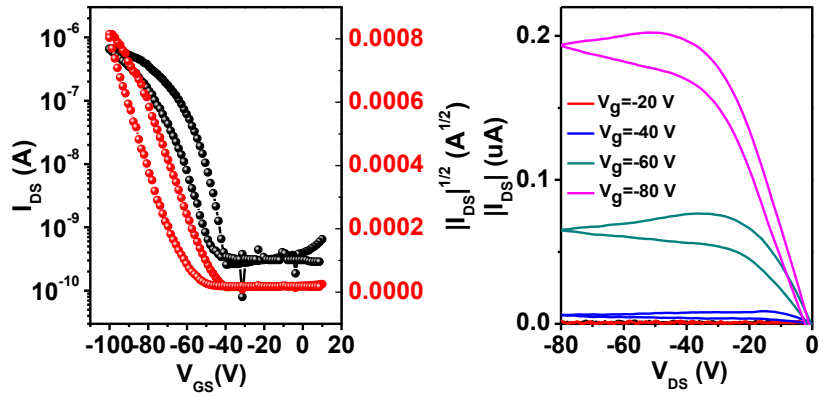

Figure S35. Transfer (left) and output (right) characteristics of **P1-OMe** thin-film based bottom-contact bottom-gate OFET (I_{DS} = source-drain current, and V_{GS} = gate voltage, V_{DS} = source-drain voltage).

9. SCLC device.

9.1 Thin film deposition and device fabrication

The indium tin oxide (ITO) glass substrate (10 Ω sq^{-1}) was cleaned by ultrasonic treatment with detergent, deionized water, acetone and ethyl alcohol for 20 min and dried with nitrogen. Then, the ITO substrate was treated with ultraviolet ozone generator for 15 min to remove organic residues. A thin film of poly(3,4-ethylenedioxythiophene):poly(styrenesulfonate) (PEDOT:PSS) was spin coated on the ITO glass substrate at 7000 rpm for 45 s and annealed on a hot plate at 140 ºC for 15 min as hole transport layer. After that, the active material (**P_1-OMe**) with a concentration of 10-20 mg/mL in trichloromethane was spin casted on PEDOT:PSS layer at 1000 rpm for 60 s and selectively annealed at 100 ºC for 10 min. At last, 100 nm of Au electrode was thermally deposited to fabricate the hole-only device. Electrical measurements (*J*-*V*) were carried out with Aglient B 1500A.

9.2 The parameter of hole-only device fabrication.

To evaluate the capability of O-doped acene as organic semiconducting materials, compound **P_1-OMe** was used as the channel material in space charge limited current (SCLC) devices. To be noted, the device fabrication is conducted in the air. With respect to a device configuration of ITO/PEDOT:PSS/**P_1-OMe**/Au, based on the Mott-Gurney equation:

$$J = \frac{9\varepsilon_0 \varepsilon \mu V^2}{8d^3}$$

where ε_0 is the vacuum permittivity, ε (~ 3) is the relative dielectric constant of active material estimated from capacitance measurements, d (~180 nm) is the film thickness, μ is hole mobility.

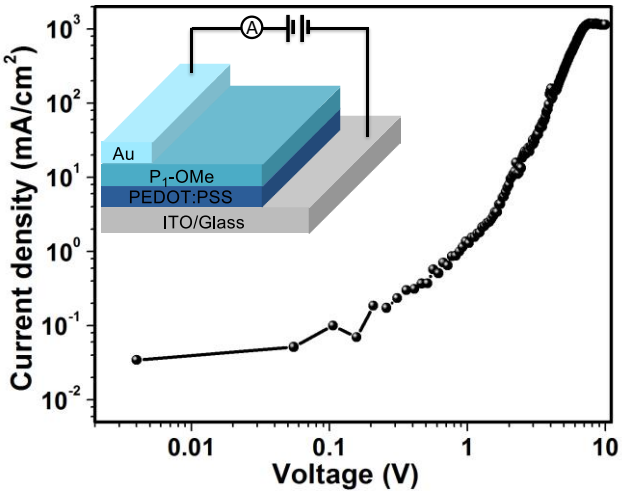

Figure S36. Measured *J-V* characteristics by the space charge limited current (SCLC) method for **P1-OMe**, the hole mobility was measured to be $\mu_h = 8.5 \times 10^{-3}$ $cm^2V^{-1}s^{-1}$.

10. NMR spectra and mass spectra for isolated compounds

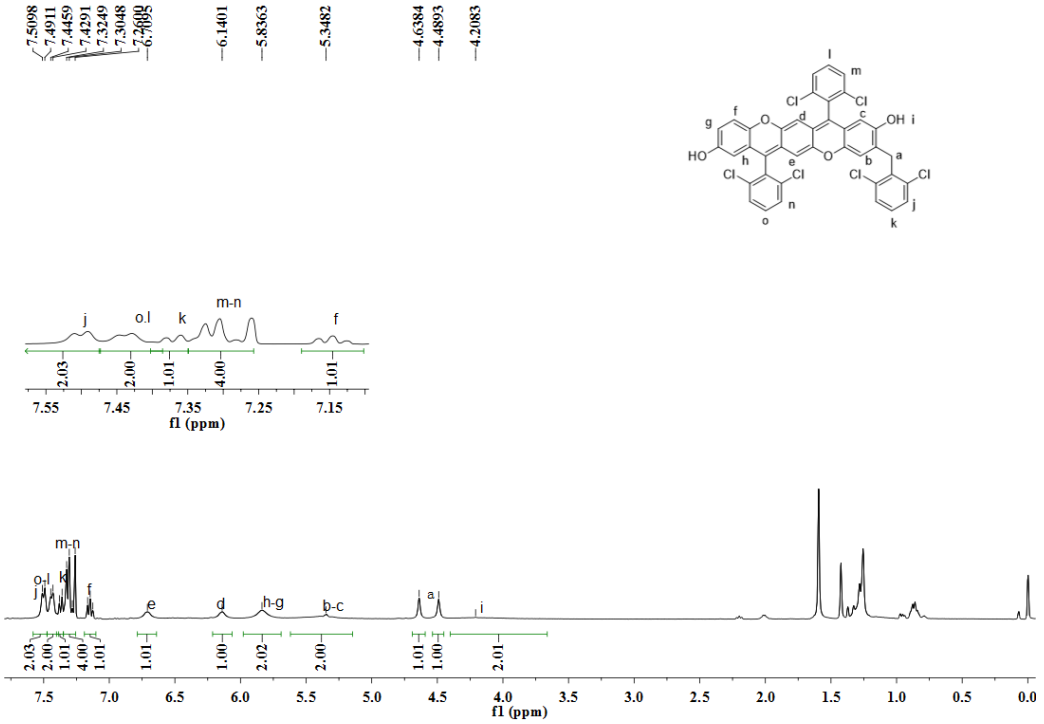

Figure S37. ^{1}H NMR spectrum (400 M) of compound **P$_1$-OH** in $CDCl_3$ at 298 K.

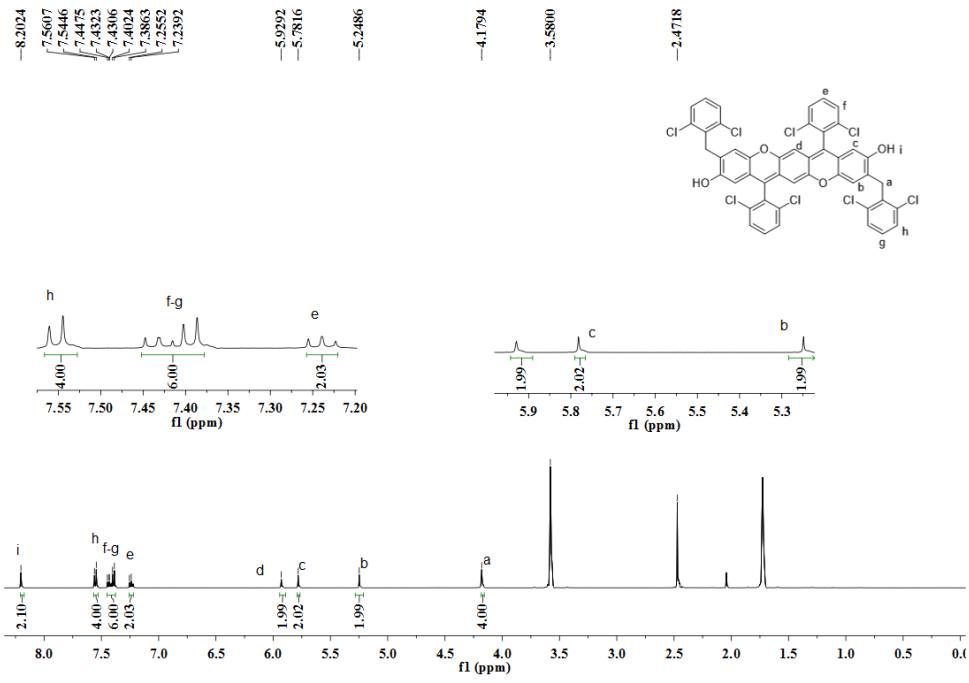

Figure S38. ^{1}H NMR spectrum (400 M) of compound **P$_2$-OH** in THF-d_8 at 298 K.

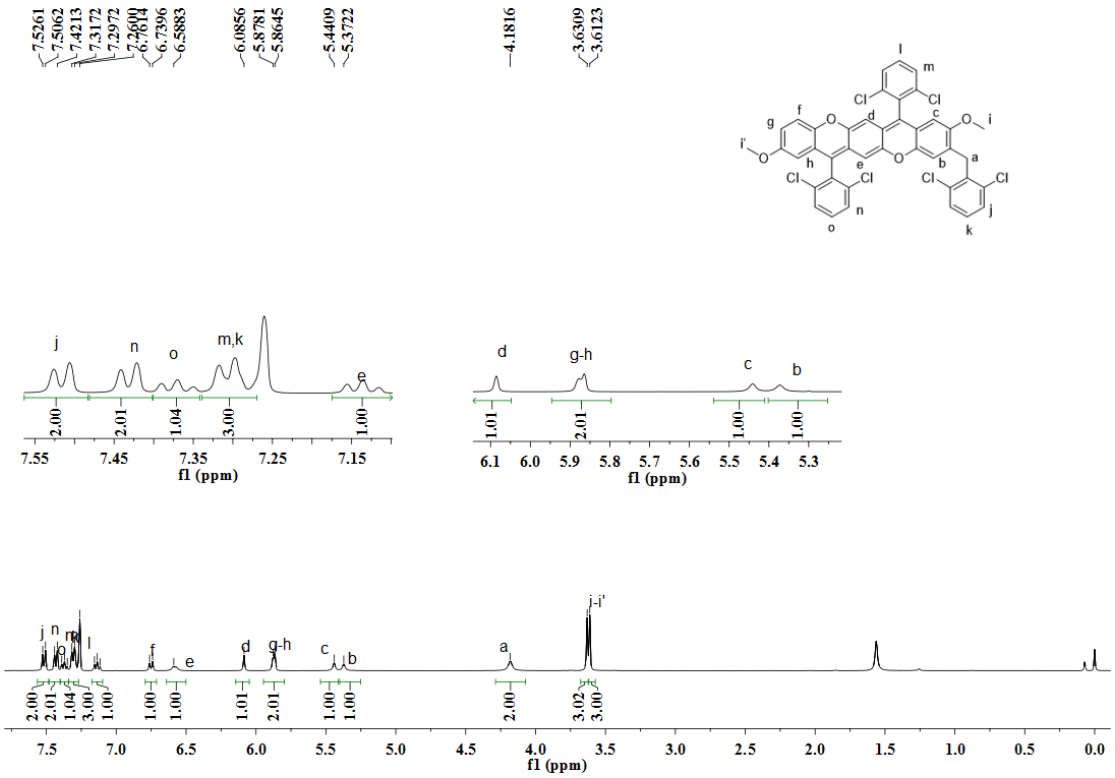

Figure S39. ^{1}H NMR spectrum (400 M) of compound **P_1-OMe** in $CDCl_3$ at 298 K.

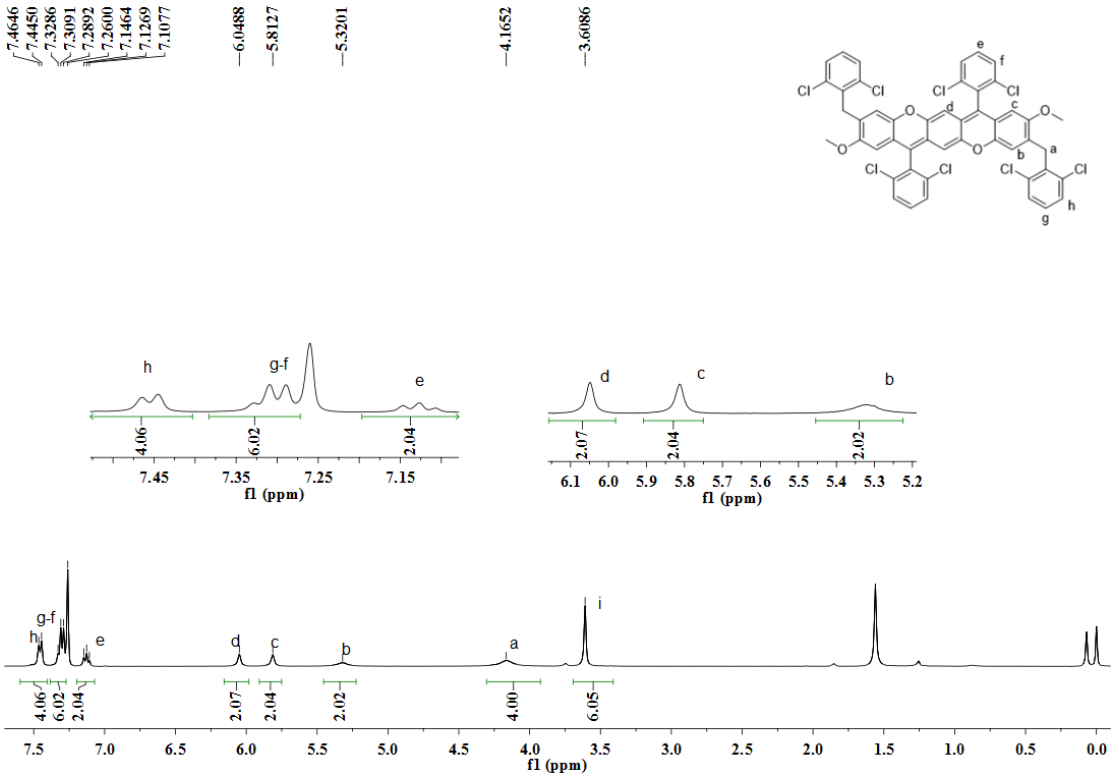

Figure S40. ^{1}H NMR spectrum (400 M) of compound **P_2-OMe** in $CDCl_3$ at 298 K.

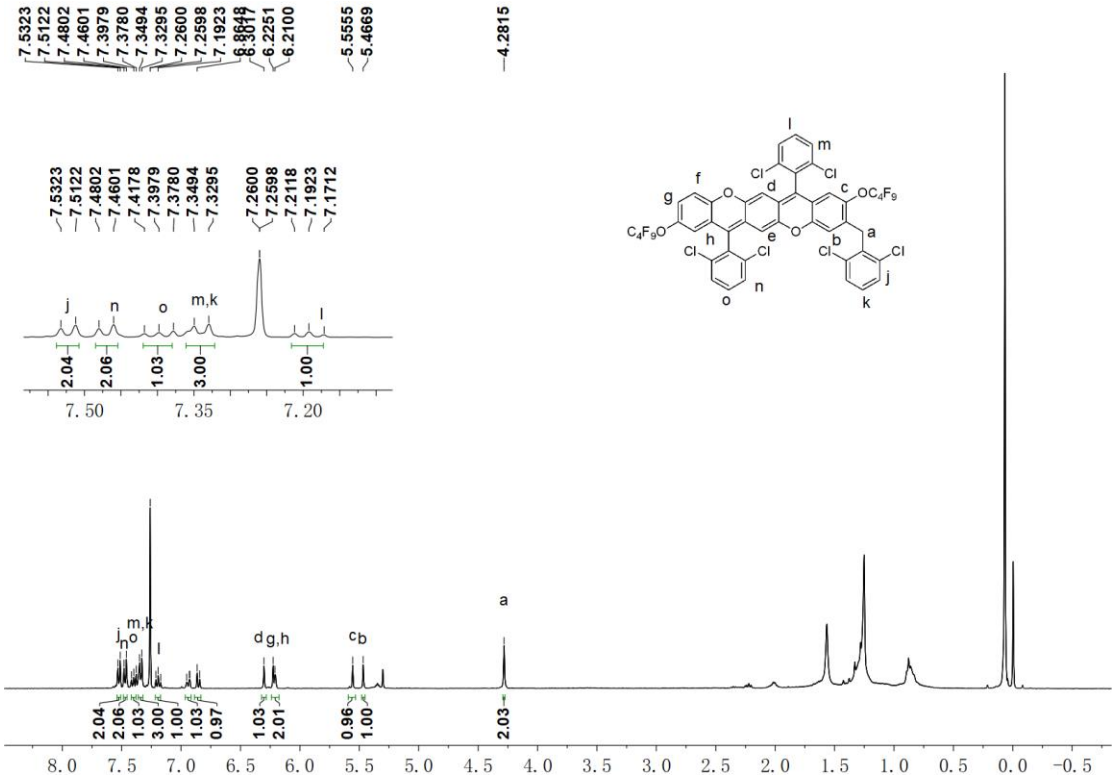

Figure S41. ^{1}H NMR spectrum (400 M) of compound **P_1-PFB** in $CDCl_3$ at 298 K.

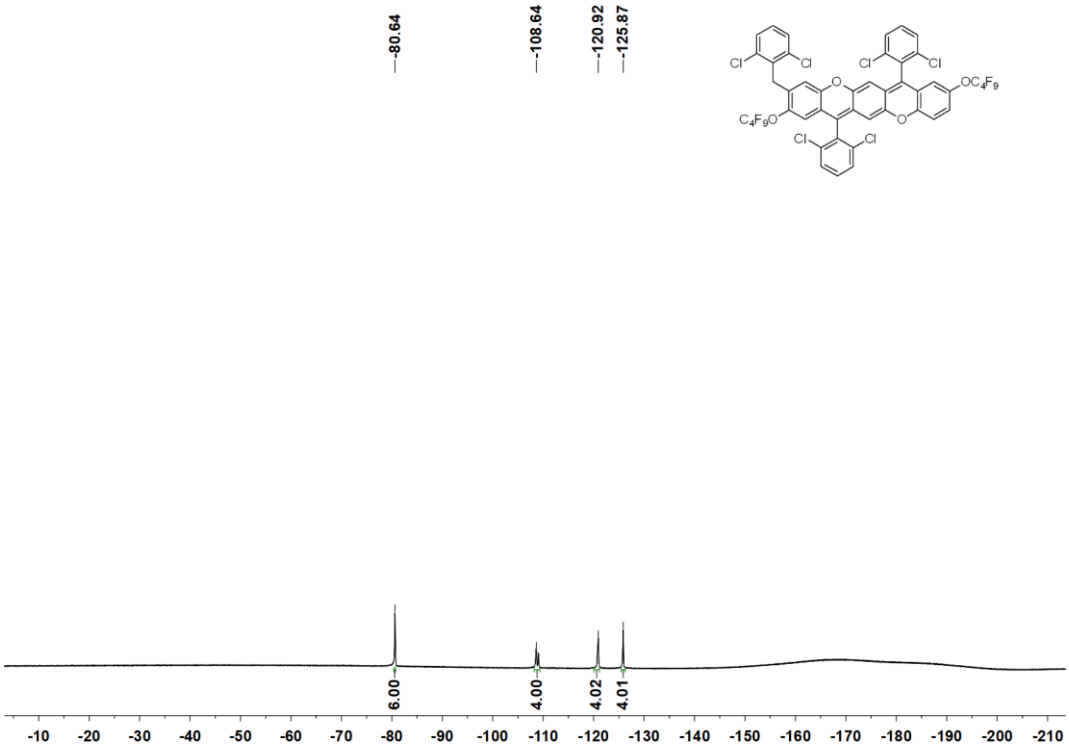

Figure S42. ^{19}F NMR spectrum (376 MHz) of compound **P_1-PFB** in $CDCl_3$ at 298K.

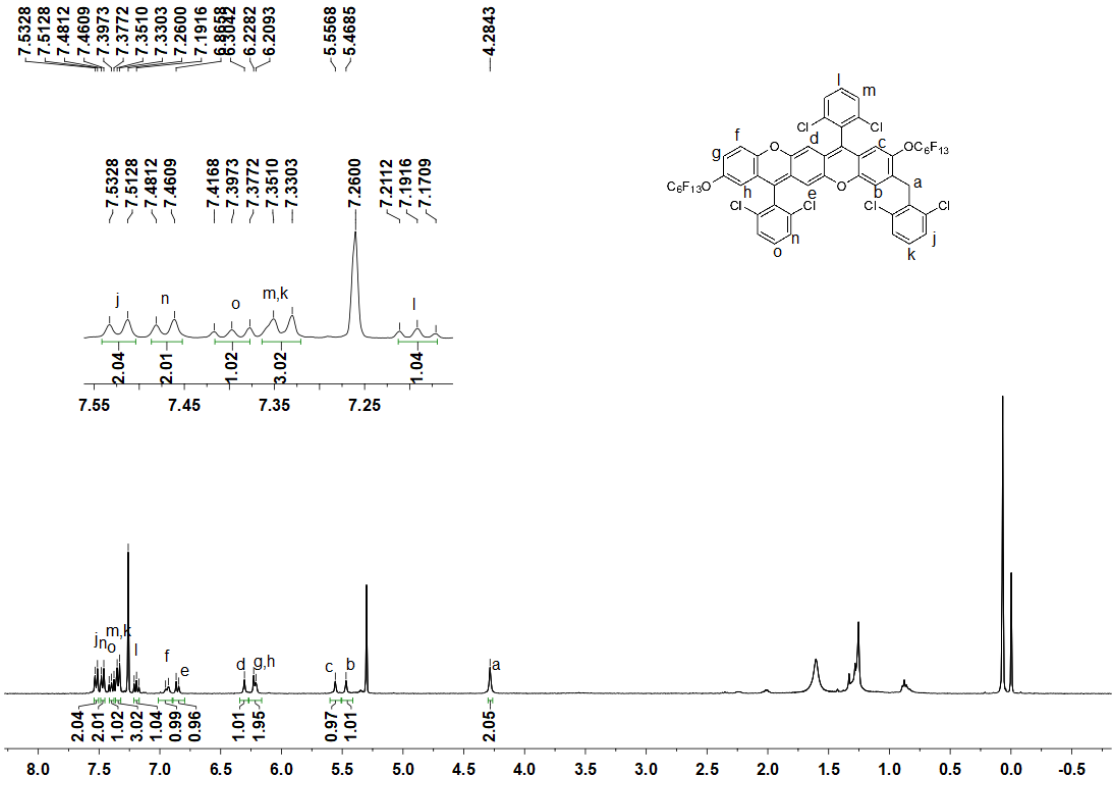

Figure S43. ^{1}H NMR spectrum (400 M) of compound **P$_1$-PFH** in $CDCl_3$ at 298 K.

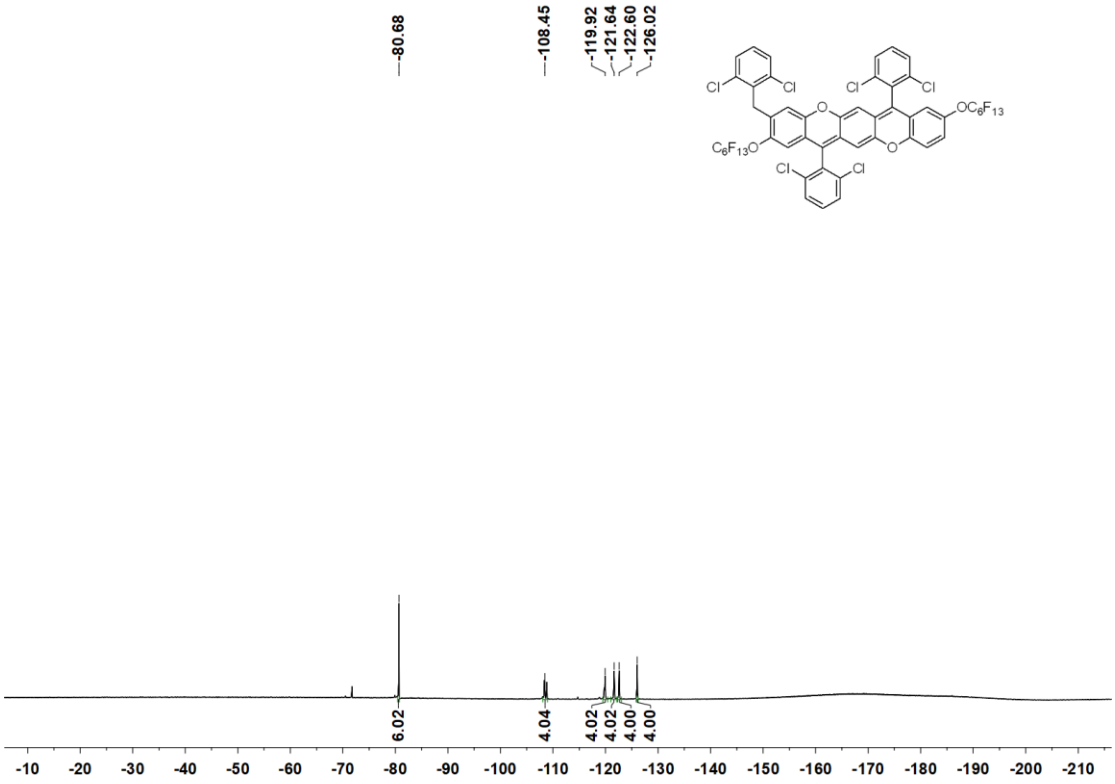

Figure S44. ^{19}F NMR spectrum (376 MHz) of compound **P$_1$-PFH** in $CDCl_3$ at 298K.

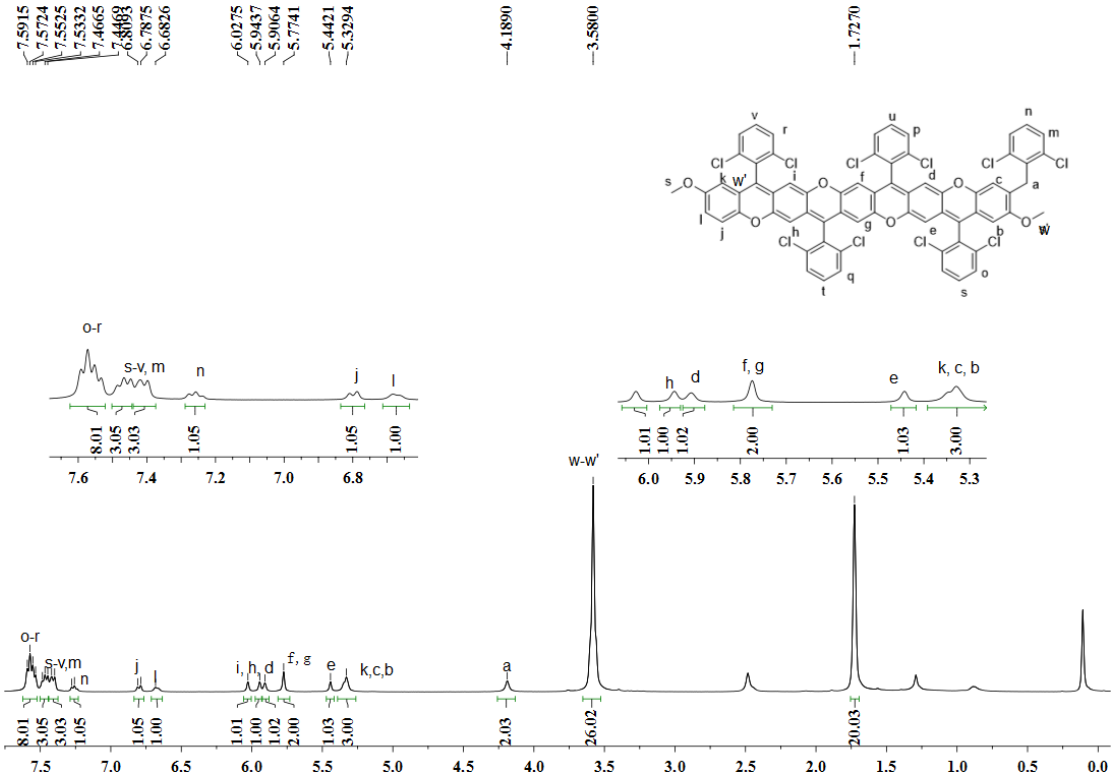

Figure S45. ^{1}H NMR spectrum (400 M) of compound **N$_1$-OMe** in THF-d_8 at 298 K.

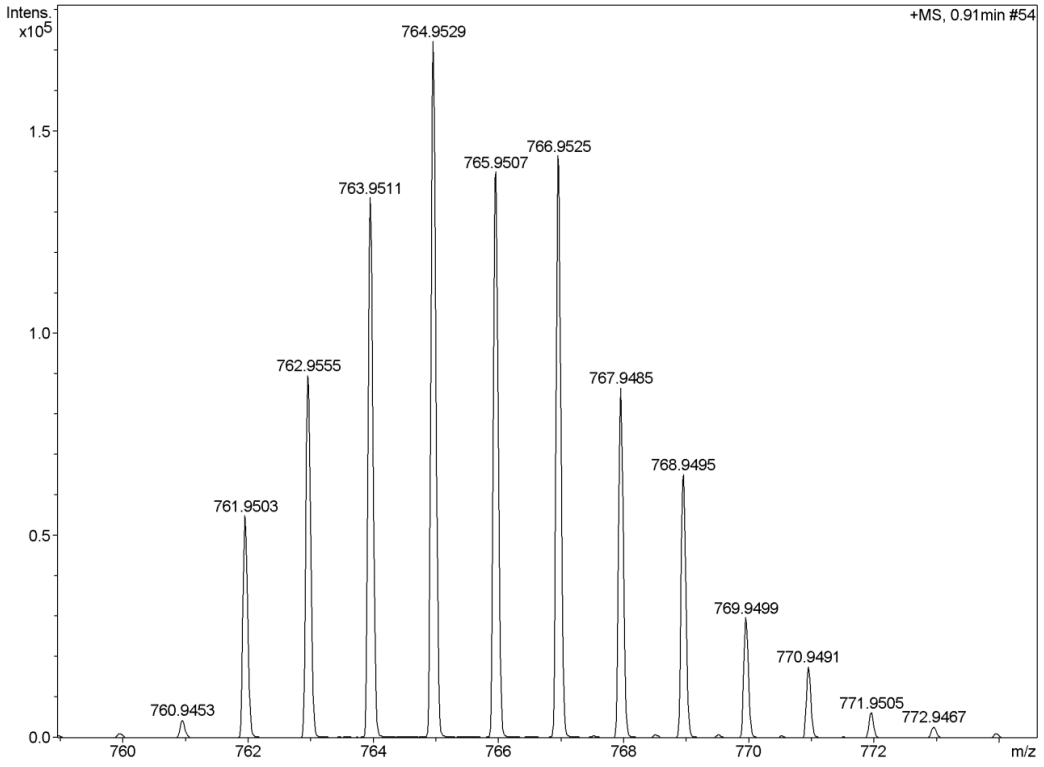

Figure S46. HR mass spectrum (APCI) of **P$_1$-OH**.

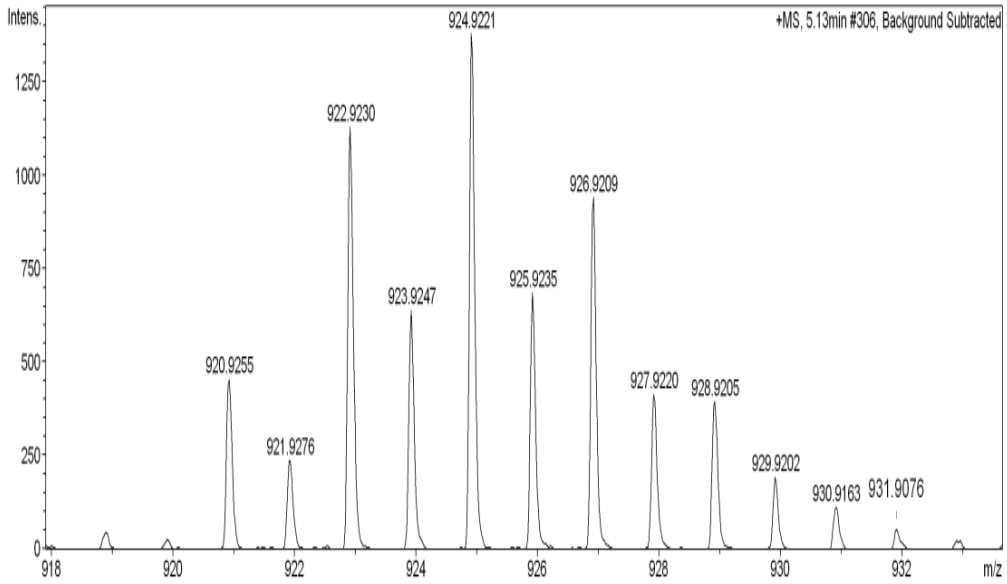

Figure S47. HR mass spectrum (APCI) of **P_2-OH**.

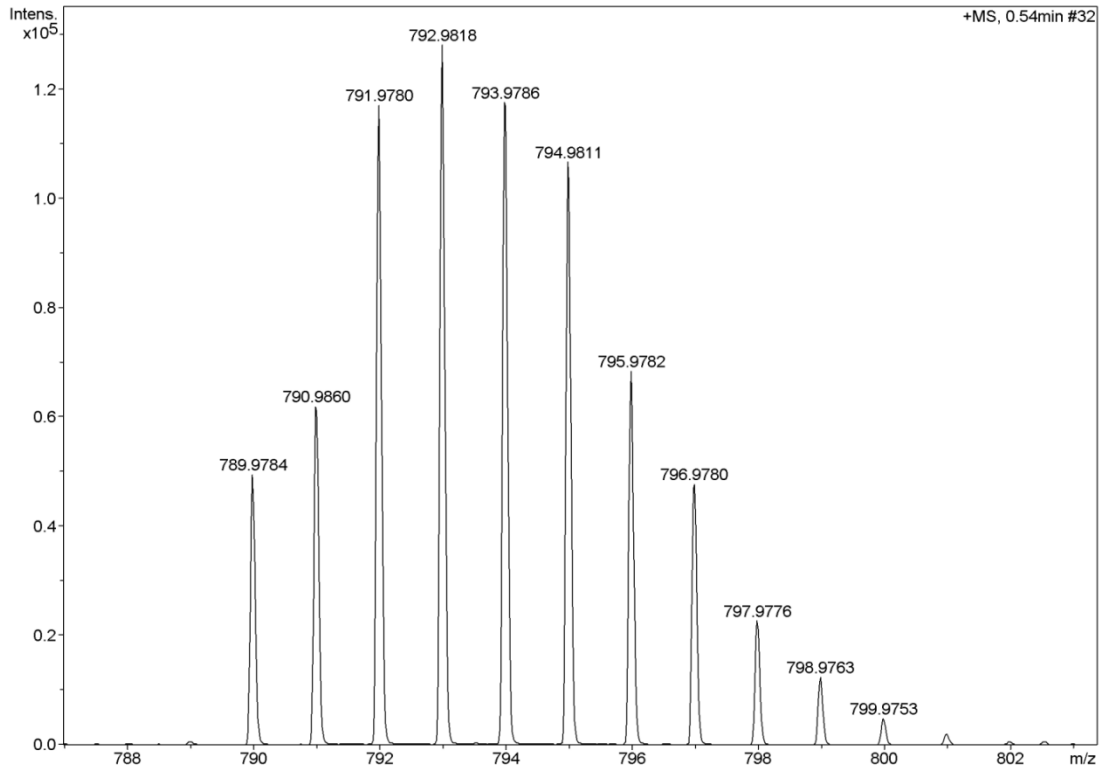

Figure S48. HR mass spectrum (APCI) of **P_1-OMe**.

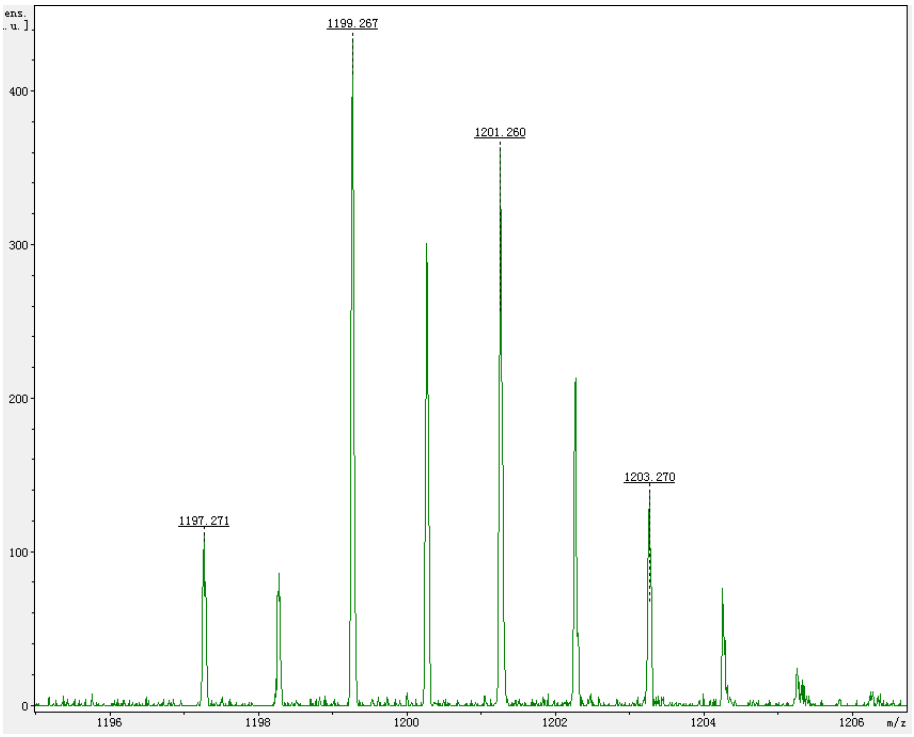

Figure S49. Mass spectrum (MALDI-TOF) of **P_1-PFB**.

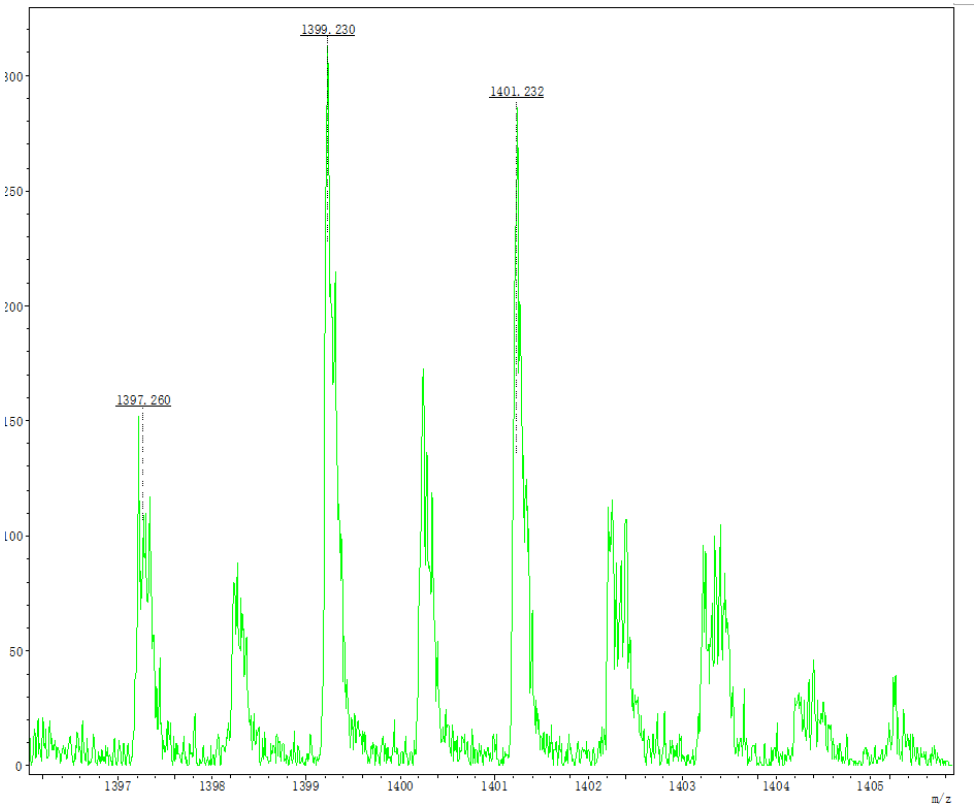

Figure S50. Mass spectrum (MALDI-TOF) of **P_1-PFH**.

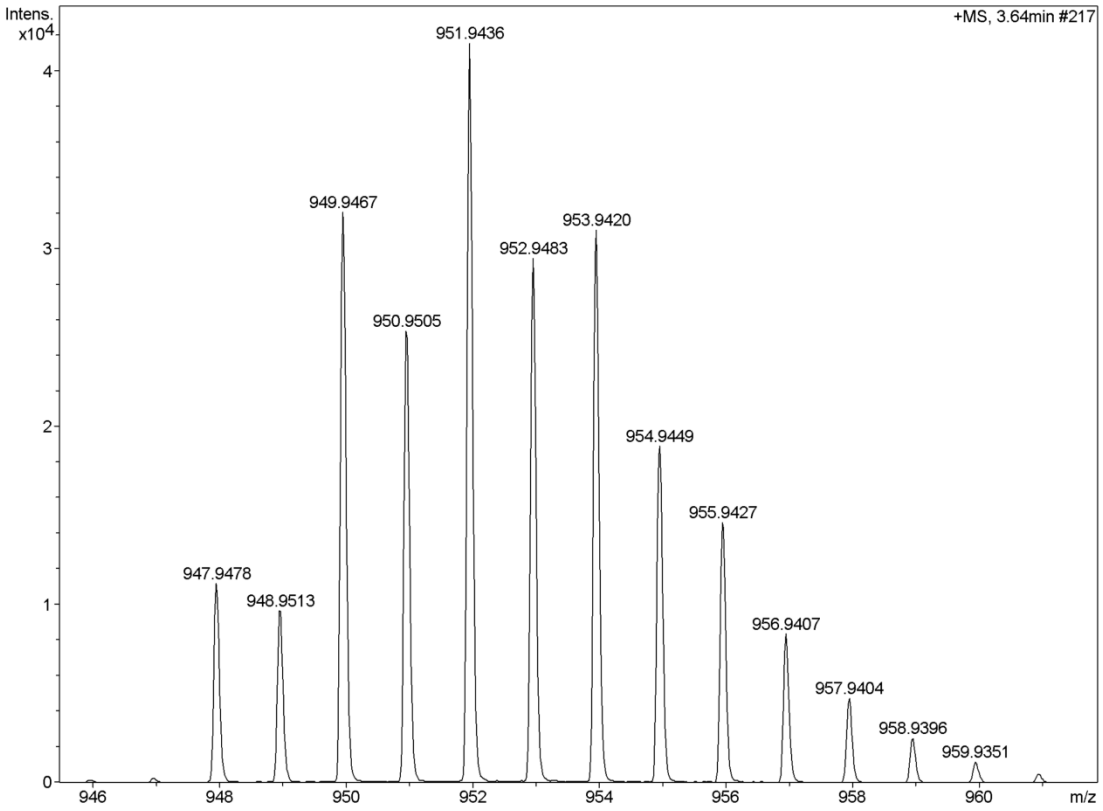

Figure S51. HR mass spectrum (APCI) of **P_2-OMe**.

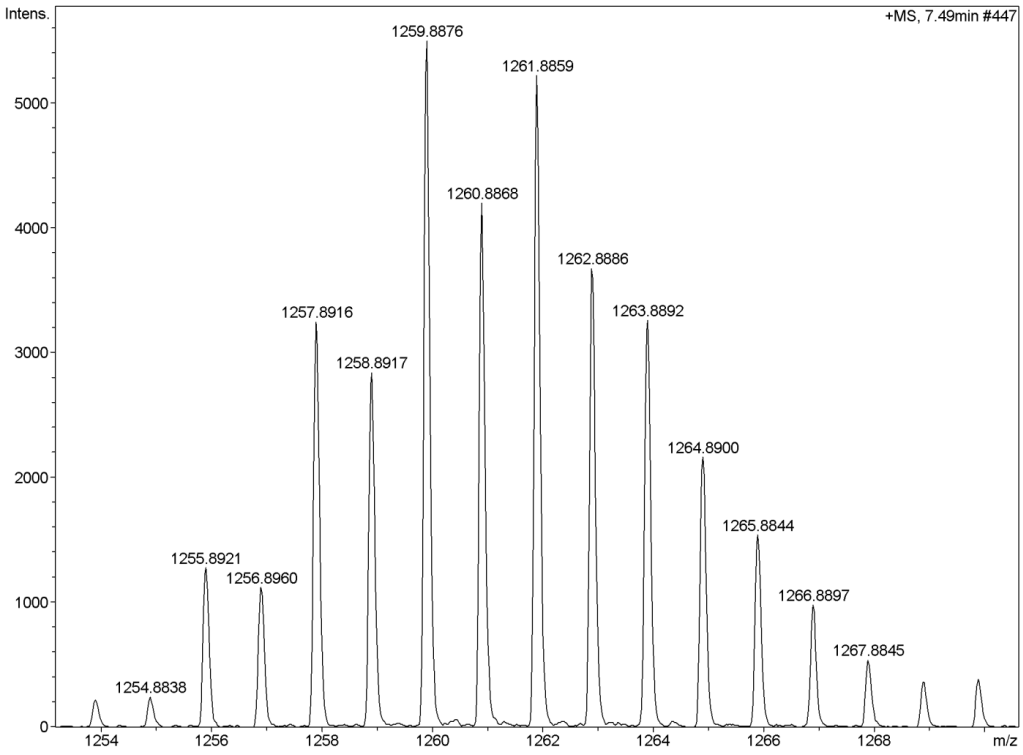

Figure S52. HR mass spectrum (APCI) of **N_1-OH**.

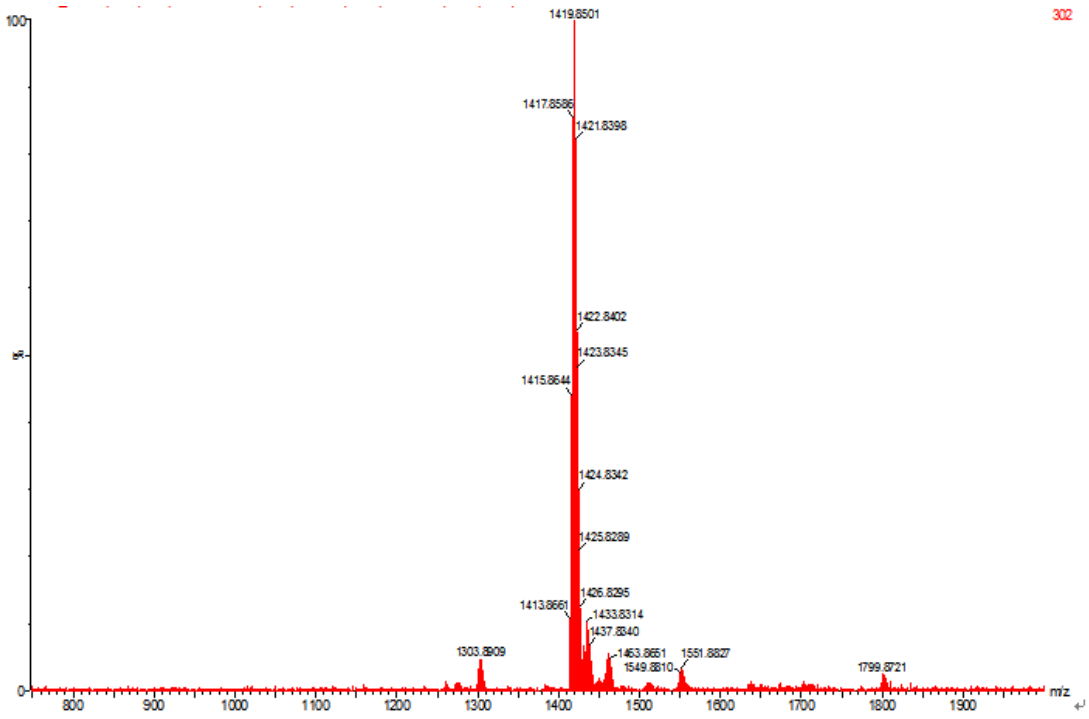

Figure S53. HR mass spectrum (MALDI-TOF) of **N_2-OH**.

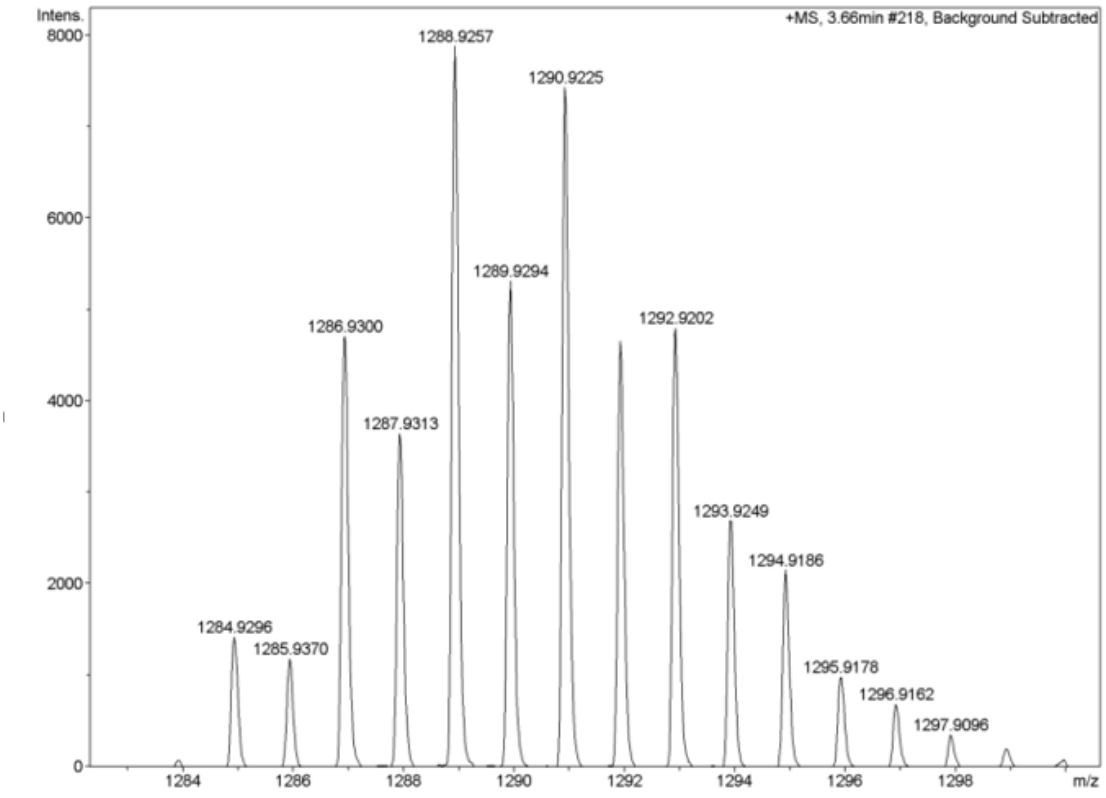

Figure S54. HR mass spectrum (APCI) of **N_1-OMe**.

References

S1. Gaussian 09, Revision C.01, Frisch, M. J.; Trucks, G. W.; Schlegel, H. B.; Scuseria, G. E.; Robb, M. A.; Cheeseman, J. R.; Scalmani, G.; Barone, V.; Mennucci, B.; Petersson, G. A.; Nakatsuji, H.; Caricato, M.; Li, X.; Hratchian, H. P.; Izmaylov, A. F.; Bloino, J.; Zheng, G.; Sonnenberg, J. L.; Hada, M.; Ehara, M.; Toyota, K.; Fukuda, R.; Hasegawa, J.; Ishida, M.; Nakajima, T.; Honda, Y.; Kitao, O.; Nakai, H.; Vreven, T.; Montgomery, Jr., J. A.; Peralta, J. E.; Ogliaro, F.; Bearpark, M.; Heyd, J. J.; Brothers, E.; Kudin, K. N.; Staroverov, V. N.; Keith, R.; Kobayashi, R.; Normand, J.; Raghavachari, K.; Rendell, A.; Burant, J. C.; Iyengar, S. S.; Tomasi, J.; Cossi, M.; Rega, N.; Millam, N. J.; Klene, M.; Knox, J. E.; Cross, J. B.; Bakken, V.; Adamo, C.; Jaramillo, J.; Gomperts, R.; Stratmann, R. E.; Yazyev, O.; Austin, A. J.; Cammi, R.; Pomelli, C.; Ochterski, J. W.; Martin, R. L.; Morokuma, K.; Zakrzewski, V. G.; Voth, G. A.; Salvador, P.; Dannenberg, J. J.; Dapprich, S.; Daniels, A. D.; Farkas, Ö.; Foresman, J. B.; Ortiz, J. V.; Cioslowski, J.; Fox, D. J. Gaussian, Inc., Wallingford CT, 2010.

S2. Zhao, Y.; Truhlar, D. G. The M06 Suite of Density Functionals for Main Group Thermochemistry, Thermochemical Kinetics, Noncovalent Interactions, Excited States, and Transition Elements: Two New Functionals and Systematic Testing of Four M06-class Functionals and 12 other Functionals. *Theor. Chem. Acc.* **2008**, 120, 215-241.